



**HAL**  
open science

## Characterization of groundwater circulations in a headwater catchment from an analysis of chemical concentrations, Sr-Nd-U isotope ratios, and CFC, SF<sub>6</sub> gas tracers (Strengbach CZO, France)

Coralie Ranchoux, François Chabaux, Daniel Viville, Thierry Labasque, Yann Lucas, Jerome van Der Woerd, Julien Ackerer, Luc Aquilina

### ► To cite this version:

Coralie Ranchoux, François Chabaux, Daniel Viville, Thierry Labasque, Yann Lucas, et al.. Characterization of groundwater circulations in a headwater catchment from an analysis of chemical concentrations, Sr-Nd-U isotope ratios, and CFC, SF<sub>6</sub> gas tracers (Strengbach CZO, France). *Applied Geochemistry*, 2021, 131, pp.105030. 10.1016/j.apgeochem.2021.105030 . insu-03261767

**HAL Id: insu-03261767**

**<https://insu.hal.science/insu-03261767v1>**

Submitted on 16 Jun 2021

**HAL** is a multi-disciplinary open access archive for the deposit and dissemination of scientific research documents, whether they are published or not. The documents may come from teaching and research institutions in France or abroad, or from public or private research centers.

L'archive ouverte pluridisciplinaire **HAL**, est destinée au dépôt et à la diffusion de documents scientifiques de niveau recherche, publiés ou non, émanant des établissements d'enseignement et de recherche français ou étrangers, des laboratoires publics ou privés.

# Journal Pre-proof

Characterization of groundwater circulations in a headwater catchment from an analysis of chemical concentrations, Sr-Nd-U isotope ratios, and CFC, SF<sub>6</sub> gas tracers (Strengbach CZO, France)

Ranchoux Coralie, Chabaux François, Viville Daniel, Labasque Thierry, Lucas Yann, Van der Woerd Jérôme, Ackerer Julien, Aquilina Luc

PII: S0883-2927(21)00162-1

DOI: <https://doi.org/10.1016/j.apgeochem.2021.105030>

Reference: AG 105030

To appear in: *Applied Geochemistry*

Received Date: 6 February 2021

Revised Date: 7 June 2021

Accepted Date: 9 June 2021

Please cite this article as: Coralie, R., François, C., Daniel, V., Thierry, L., Yann, L., Jérôme, V.d.W., Julien, A., Luc, A., Characterization of groundwater circulations in a headwater catchment from an analysis of chemical concentrations, Sr-Nd-U isotope ratios, and CFC, SF<sub>6</sub> gas tracers (Strengbach CZO, France), *Applied Geochemistry*, <https://doi.org/10.1016/j.apgeochem.2021.105030>.

This is a PDF file of an article that has undergone enhancements after acceptance, such as the addition of a cover page and metadata, and formatting for readability, but it is not yet the definitive version of record. This version will undergo additional copyediting, typesetting and review before it is published in its final form, but we are providing this version to give early visibility of the article. Please note that, during the production process, errors may be discovered which could affect the content, and all legal disclaimers that apply to the journal pertain.

© 2021 Elsevier Ltd. All rights reserved.



1 **Characterization of groundwater circulations in a headwater catchment from**  
2 **an analysis of chemical concentrations, Sr-Nd-U isotope ratios, and CFC, SF<sub>6</sub>**  
3 **gas tracers (Strengbach CZO, France)**

4  
5  
6 Ranchoux Coralie<sup>1,3</sup>, Chabaux François<sup>1\*</sup>, Viville Daniel<sup>1</sup>, Labasque Thierry<sup>2</sup>, Lucas Yann<sup>1</sup>, Van der  
7 Woerd Jérôme<sup>1</sup>, Ackerer Julien<sup>1,4</sup>, Aquilina Luc<sup>2</sup>

8 1- Institut Terre et Environnement Strasbourg (ITES), formerly: Laboratoire d'Hydrologie et de Géochimie de  
9 Strasbourg (LHyGeS) , Université de Strasbourg, CNRS, ENGEEES, 67000 Strasbourg, France.

10 2- Geosciences Rennes, CNRS, Université Rennes 1, 35000 Rennes, France.

11 3- Present address : HydroSciences Montpellier, Montpellier University, CNRS, IRD, 34000 Montpellier, France

12 4- Present address : Institut des Géosciences de l'environnement, CNRS, Université Grenoble Alpes, Grenoble INP,  
13 IRD, 38000 Grenoble, France.

14  
15 \*Correspondence : [fchabaux@unistra.fr](mailto:fchabaux@unistra.fr), [cora.ranch@hotmail.fr](mailto:cora.ranch@hotmail.fr)

16  
17  
18  
19 **Keywords:** Sr, Nd, and U isotopic ratios; CFC-SF<sub>6</sub> concentrations; groundwater age dating; water-rock  
20 interactions; Strengbach CZO.

21 **Abstract:** 265 words

22 **Main text:** 9,701 words

**23 Abstract**

24 In order to characterize the chemical composition and the age of the water circulating in the critical  
25 zone of the Strengbach catchment (Vosges mountains, France), water samples from springs, 10–15 m  
26 deep piezometers and 50–120 m deep boreholes were collected and analyzed in elementary  
27 concentrations, in Sr, Nd, and U isotopic ratios, and in chlorofluorocarbon (CFC) and sulfur  
28 hexafluoride ( $\text{SF}_6$ ) concentrations. The results evidence a clear distinction between surface water (<  
29  $\approx 10$ -15 m) and deeper water. The latter has much higher conductivity and cationic loads and is  
30 marked by lower Sr isotopic ratios and higher U activity ratios. Such a water typology suggests that  
31 the spring and piezometer water flows within the same shallow subsurface aquifer while deep  
32 borehole water belongs to a different circulation system, which flow path is controlled by the  
33 bedrock fracture network. The CFC data show that these two circulation systems are marked by  
34 contrasted residence times with a short residence time for the surface water and a longer residence  
35 time (water ages > 50 years) for the deep water. These results confirm different circulation histories  
36 for surface and deep water in the Strengbach catchment. They also suggest that the higher degree of  
37 chemical saturation of the deep water compared to the surface water is caused more by longer  
38 water residence times in the deep circulation systems than by differences in the primary minerals  
39 involved in each of the water-rock interaction systems. Our results also point that in the Strengbach  
40 granitic catchment, the  $\text{SF}_6$  concentrations cannot be used for water dating due to their lithogenic  
41 production in granitic bedrocks.

42

43

## 44 1. Introduction

45 The identification of the main water circulation levels in the Critical Zone (CZ) and the  
46 determination of the characteristic times of these circulations are among key parameters controlling  
47 the CZ functioning and its vertical extension (i.e., Riebe et al., 2017). These parameters also control  
48 its future evolution in response to environmental modifications, whether related to global climate  
49 change or to human activities of more local impact. This information, in particular, the partitioning  
50 between deep and subsurface circulations, is also important to achieve a sustainable management of  
51 the world's water resources and to model their future evolution in response to ongoing climate  
52 change (e.g., Gleeson et al., 2016; Ameli et al., 2017; Liu et al., 2017; O'Geen et al., 2018; Weill et al.,  
53 2019; Ackerer et al., 2020a).

54 Surface and subsurface water circulations, especially in small headwater watersheds, are  
55 studied more than deep water circulations occurring in fractured bedrock (e.g., Viville et al., 2012;  
56 Brantley et al., 2017). The relatively recent setting up of several tens of meters-deep boreholes on  
57 such watersheds, especially those belonging to the so-called Critical Zone Observatories, is now  
58 allowing a much better exploration of water circulations and weathering processes in the deeper  
59 parts of the CZ (e.g., Brantley et al., 2013; Buss et al., 2013; Chabaux et al., 2017; Hahm et al., 2019;  
60 Holbrook et al., 2019; Ranchoux, 2020). These latter studies have systematically evidenced water  
61 circulation at great depths in the various explored sites. The hydrogeochemical characteristics of  
62 these waters, in particular, their specificity compared to surface waters, should be further clarified to  
63 better identify the water-rock interaction processes occurring in the deep CZ and the water  
64 circulation residence times in these deep levels.

65 The purpose of this study, conducted on the Strengbach CZO, France, is to determine the  
66 nature and residence time of the various waters circulating in the bedrock of the Strengbach  
67 catchment from the surface to  $\approx 100$ m depth. The Strengbach basin has been the subject of relatively  
68 extensive hydrogeochemical studies in the past for surface waters (springs, soil solutions, streams),

69 which today allows us to have a fairly good knowledge of their geochemical composition in major  
70 elements as well as Sr, Nd, and U isotopic ratios. These elements and ratios are relevant tracers when  
71 we seek to decipher the main water-rock interactions involved in biogeochemical and  
72 hydrogeochemical cycles (e.g., Aubert et al., 2001; Riotte and Chabaux, 1999; Tricca et al., 1999;  
73 Chabaux et al., 2011, 2013, 2019; Durand et al., 2005; Schaffhauser et al., 2014; Pierret et al., 2014,  
74 and references therein). All these data have led us to propose a first order relatively solid  
75 interpretative framework on the nature of water-rock interactions controlling the geochemical  
76 composition of surface waters in the Strengbach catchment.

77 In the current study, we propose to establish the hydrogeochemical typology of the deeper  
78 waters of the Strengbach CZO by a multi-method geochemical approach that combines the analysis  
79 of the above tracers (i.e., major and trace elements, Sr, Nd, and U isotope ratios) with the analysis of  
80 anthropogenic gases, namely, chlorofluorocarbons (CFCs) and sulfur hexafluoride (SF<sub>6</sub>). These latter  
81 elements are indeed suitable for determining the water ages and/or residence times in aquifers for  
82 relatively recent periods, 0-70 years or a little more, depending on the interpretative models used  
83 (e.g., Busenberg and Plummer, 1992; Corcho Alvarado et al., 2005; Plummer et al., 1998; Jankovec et  
84 al., 2017; De Montety et al., 2018; Cao et al., 2020). In particular, anthropogenic gases were  
85 successfully applied to estimate mean water transit time in fractured aquifers (Cook et al., 1996,  
86 2005; Plummer et al., 2000; Bockgard et al., 2004; Ayraud et al., 2008; Jaunat et al., 2012; Roques et  
87 al., 2014a, b; Marçais et al., 2018). The results presented here on the Strengbach CZO highlight the  
88 interest of combining these different geochemical tracers to explore the hydrological functioning of  
89 the deep CZ.

90

91

## 92 2. Site presentation

93 The Strengbach catchment is a small 0.8 km<sup>2</sup> granitic catchment in the Vosges mountains  
94 (northeastern France) at an altitude ranging between 880 and 1150 m a.s.l. with fairly steep slopes  
95 (mean slope of 15°) (Fig. 1). It is an equipped environmental observatory where meteorological,  
96 hydrological, and geochemical data have been recorded since 1986 (Observatoire Hydrologique et  
97 Géochimique de l'Environnement/Hydrological and Geochemical Environmental Observatory, OHGE;  
98 <http://ohge.unistra.fr>) and is one of the reference headwater sites of the French critical zone  
99 observatory network OZCAR (Observatoire de la Zone Critique: Application et Recherche/ Critical  
100 Zone Observatories: Research and Application, <https://www.ozcar-ri.org>). The climate is temperate  
101 oceanic mountainous with a mean annual temperature of 7 °C (mean monthly from -2 to 14 °C).  
102 Annual precipitation is between 890 to 1630 mm.yr<sup>-1</sup> (mean 1400 mm.yr<sup>-1</sup>) with snow cover for 2-4  
103 months.yr<sup>-1</sup> (Viville et al., 2012; Pierret et al., 2014). The mean runoff of the catchment is 853 mm and  
104 varies from 525 to 1147 mm (Ladouche et al., 2001; Viville et al., 2012). Forest covers 90% of the  
105 surface area (Azaël, 1990) and is essentially composed of 80% spruce trees and 20% beech trees.

106 The bedrock is mainly constituted by a Hercynian leucogranite affected by hydrothermal  
107 alteration (e.g., Fichter et al., 1998a, b; Chabaux et al., 2019). The hydrothermal events caused the  
108 alteration and transformation of primary minerals (albite, K-feldspars, muscovite) into fine-grained  
109 illite and quartz. There is an occurrence of gneiss in the upper part of the northern slope of the basin  
110 (El Gh'mari, 1995; Fichter, 1997; Fichter et al., 1998; Chabaux et al., 2019). Compared to granitic  
111 bedrocks, gneiss is enriched in Mg due to the presence of biotite and chlorite (El Gh'mari, 1995;  
112 Fichter, 1997). The soils are 80–100 cm deep and vary from Dystric Cambisol (southern slope) to Albic  
113 Podzol (northern slope). The soils are usually developed on a sandy saprolite, 1 to 9 m thick, the  
114 thickest saprolite being located on the downstream part of the southern slope (El Gh'mari, 1995).  
115 Several springs are emerging in the catchment on both slopes. Some of them (Cs1, Cs2, Cs3, Cs4,  
116 ARG, RH3) were sampled for the present study (location on Fig. 1).

117 For studying deep water circulation within the Strengbach watershed, the site was equipped,  
118 between 2012 and 2014, with 9 boreholes drilled along two transects, one along the south-facing  
119 slope, and one along the north-facing slope (Fig. 1c-d). This includes six deep boreholes (50 to 120 m  
120 depth — F1a,b, F5, F6, F7, F8) and three shallower ones of  $\approx 15$  m depth (pz3, pz5, pz7), named  
121 piezometers in the following text. The main equipment installed in each well is summarized in  
122 Supplementary Material Table 1 (SM Table1). Briefly, the three piezometers were equipped along  
123 their length with a PVC tube, cased for the first two meters and screened deeper. In the screened  
124 zones, gravel pack was introduced between the tube and the bedrock. Boreholes F6, F7, and F8,  
125 drilled in 2012, were entirely cased and equipped with multi-level screened sections (SM Table 1), in  
126 front of well-located fracture zones identified by the drilling company and considered as potential  
127 water circulation levels. A gravel pack was set up outside the screened sections to ensure proper  
128 water flow, and clay plugs of bentonite (compactonite) were used to tighten the cased sections. To  
129 limit the pollution risks of the chemical composition of the water by the gravel and bentonite used in  
130 the above wells, it was decided to equip the southern slope with uncased wells. Thus, boreholes F5  
131 and F1, drilled in 2013 and 2014, are uncased holes throughout their depth, except for the first 8 m  
132 where a PVC casing and a cement sheath were installed.

133

### 134 **3. Methodology**

#### 135 **3.1 Water sampling procedure**

136 For the present study, 10 sampling campaigns, covering the diversity of hydrological contexts  
137 encountered on the catchment, were conducted over the period 05/2015–10/2018 (Fig. 2) for  
138 collecting water from springs CS1, CS2, CS3, CS4, RH3, and ARG, piezometers pz3, pz5, and pz7, and  
139 deep boreholes F5, F6, F7, and F8. Piezometer and borehole water were sampled with a pump  
140 descended to the chosen depth after generally 10 min of pumping, which is the time required to  
141 renew the water in the well. Piezometers were sampled at a depth of between 10 to 14 m. For deep  
142 borehole water, the initial sampling depths corresponded to the depths at which more significant

143 fractures were noticed from acoustic and optical logging. The sampling depths were adapted during  
144 the course of the study based on the first conductivity logging obtained in the wells as explained in  
145 Ranchoux (2020) (see Table 1 for sampling dates, sample depths, and the analyses performed on  
146 each sample).

147 Samples collected for major and trace element concentrations and Sr-Nd-U isotopic analyses  
148 were stored in 2 L polypropylene bottles, which were previously cleaned with ultra-pure HCl and  
149 ultra-pure water (18.2 MΩ.cm). For some Nd analyses requiring larger water volumes (up to 10 to 15  
150 L), water was stored in large food-grade PVC water tanks. For analysis of dissolved gas concentrations  
151 (Ar, Ne, N<sub>2</sub>, O<sub>2</sub>) and CFC and SF<sub>6</sub> concentrations in water, samples were collected following the  
152 procedure described in Labasque et al. (2004, 2014). Water samples were stored in 500 mL glass  
153 bottles for Ar, Ne, N<sub>2</sub>, and O<sub>2</sub> measurements and in steel ampoules of 40 ml and 300 ml for CFC and  
154 SF<sub>6</sub> analyses, respectively.

155

### 156 **3.2 Analysis of major element concentrations and Sr-Nd-U isotope ratios**

157 Determination of major and trace element concentrations, Sr-Nd isotope ratios, and U activity  
158 ratios were performed at LHyGeS, Strasbourg, France. Water samples were filtered through a 0.45  
159 μm cellulose acetate membrane filter. Each water sample was divided into two aliquots. One aliquot  
160 was acidified with bidistilled 13.5 N HNO<sub>3</sub> to pH≈1 for trace element and isotopic analyses. The other  
161 aliquot was not acidified, measured pH and conductivity, and analyzed major element and Dissolved  
162 Organic Carbon (DOC) concentrations, following the standard procedures used in the laboratory (e.g.,  
163 Lucas et al., 2010; Schaffhauser et al., 2014; Gangloff et al., 2014; Prunier et al., 2015). The pH was  
164 determined using a Meterlab® PHM210 pH-meter with a precision of ±0.02 units and the  
165 conductivity using a Meterlab® CDM210 conductometer with an uncertainty from 1 to 2%. The DOC  
166 was measured by the thermal method (Shimadzu TOC VPH ) with an uncertainty of 2% and a  
167 detection limit of 0.3 mgC L<sup>-1</sup>. Cation (Na<sup>+</sup>, K<sup>+</sup>, NH<sub>4</sub><sup>+</sup>, Ca<sup>2+</sup>, and Mg<sup>2+</sup>) and anion (Cl<sup>-</sup>, SO<sub>4</sub><sup>2-</sup>, and NO<sub>3</sub><sup>-</sup>)  
168 concentrations were analyzed by ionic chromatography (ICS 5000 Thermo Scientific) with

169 uncertainties of 2% and a detection limit of  $5\mu\text{mol}\cdot\text{L}^{-1}$ . The Al, Mn, P, Si, and Fe concentrations were  
170 measured by ICP-AES (Inductively Coupled Plasma Atomic Emission Spectrometry) with a Thermo  
171 ICAP 6500, a detection limit of  $1\mu\text{g}/\text{l}$ , and a measurement uncertainty of  $\approx 5\%$ . Trace element  
172 concentrations were analyzed by ICP-MS (Inductively Coupled Plasma Mass Spectrometer) Thermo  
173 XseriesII with an uncertainty of  $\approx 5\%$  and detection limits between 1–10 ppt, depending on the  
174 elements.

175  $(^{234}\text{U}/^{238}\text{U})$  activity ratios were analyzed by mass spectrometry on a Neptune Thermo-Scientific  
176 multi-collector (MC-ICP-MS). U was first separated and purified by anionic exchange chromatography  
177 following procedures developed at the LHyGeS (e.g., Chabaux et al., 1995; Riotte and Chabaux,  
178 1999). The procedure blanks were  $<10\text{ pg}$ , negligible compared to the U amount processed. The  
179 reproducibility and reliability of the U isotopic analysis were tested by the regular measurement of  
180 the HU1 standard, assumed to be in secular equilibrium, which for the analysis period 2015–2018  
181 gave a  $(^{234}\text{U}/^{238}\text{U})$  activity ratio of  $0.999 \pm 0.003$  (2SD,  $n = 71$ ).

182 For Sr and Nd isotope measurements, Sr and Nd were extracted and purified following the  
183 chromatography procedures used in the laboratory (Geagea et al., 2007; Guéguen et al., 2012). For  
184 Nd analysis on large water volume ( $>1\text{L}$ ), Nd was first extracted from the water by coprecipitation  
185 with  $\text{Fe}(\text{OH})_3$ , followed by iron removal on cation exchange resins (Chauvel et al., 2011; Pelt et al.,  
186 2013).  $^{87}\text{Sr}/^{86}\text{Sr}$  and  $^{144}\text{Nd}/^{143}\text{Nd}$  isotope ratios were measured on a Neptune Thermo-Scientific  
187 multicollector (MC-ICP-MS) and Thermo-Scientific Triton Thermal Ionisation Mass Spectrometry  
188 (TIMS), respectively. Blanks were  $<1\text{ng}$  for Sr, i.e., negligible compared to the Sr amount analyzed in  
189 the samples. For Nd they reached  $130\text{ pg}$  for samples processed with a coprecipitation stage, which  
190 represented a maximum contribution of 2-3% of the Nd used for the analysis in the few samples  
191 where the Nd amount processed was between 5 and 10 ng. The regular analysis of SRM 987 standard  
192 for the analysis period 2015-2018 gave a  $^{87}\text{Sr}/^{86}\text{Sr}$  isotope ratio  $0.71026 \pm 0.00003$  (2SD,  $n = 41$ ).  
193 Analysis of the La Jolla standard gave a  $^{144}\text{Nd}/^{143}\text{Nd}$  isotope ratio of  $0.511846 \pm 0.00002$  (2SD,  $n = 39$ )

194 for a Nd amount processed > 10 ng and a ratio of  $0.511846 \pm 0.00004$  (2SD, n = 8) for a Nd amount  
195 between 2 and 10 ng.

196

### 197 **3.3 Analysis of CFC, SF<sub>6</sub>, and noble gas concentrations**

198 The CFC, SF<sub>6</sub>, and dissolved gas were analyzed at the Condate Eau platform (OSUR, University  
199 of Rennes, France). CFC and SF<sub>6</sub> were extracted by purge and trap and measured by gas  
200 chromatography with electron capture detection (Labasque, 2004), modified from Busenberg and  
201 Plummer methodology (1992, 2000). An uncertainty of 4% applies for high concentrations (above 0.1  
202 pmol/kg for CFC and 0.1 fmol/kg for SF<sub>6</sub>) and rises to 20% for lower values, next to the detection limit  
203 (between 0.01 to 0.05 pmol/L for CFC and 0.06 fmol/L for SF<sub>6</sub>) (Labasque et al., 2006; Labasque et al.,  
204 2014). Samples for dissolved gases (Ar, Ne, N<sub>2</sub>, O<sub>2</sub>) were analyzed by gas chromatography following  
205 the Sugisaki method (Sugisaki and Taki, 1987) at the Condate Eau platform with uncertainties of  
206 around 3% for minor gases (< 100 ppm) and 1% for others.

207

### 208 **3.4 Residence time and ages estimation model**

209 CFC and SF<sub>6</sub> water concentrations were converted to atmospheric partial pressure (pptv) to be  
210 interpreted in terms of residence time by comparing these atmospheric concentrations with  
211 theoretical values obtained in simple hydrological models classically used for dating purposes. The  
212 conversion was done using the solubility functions for CFC-11, CFC-12, CFC-113, and SF<sub>6</sub> provided by  
213 Warner and Weiss (1985), Bu and Warner (1995) and Bullister, et al. (2002), respectively. Results  
214 obtained in such conversion depend on recharge temperature, altitude, and excess air (Darling et al.,  
215 2012). For the present study, the excess air was calculated using Ne concentrations, following the  
216 approach given in Heaton and Vogel (1981). The mean recharge temperature was fixed at 7 °C, the  
217 mean annual temperature measured at the meteorological station located at one of the summits of  
218 the Strengbach watershed (Fig. 1 for location). The recharge altitude used was consequently taken to  
219 1100 m, the ≈ altitude of the meteorological station. The dependence of the results on the selected

220 recharge altitude and temperature is about 1.3%/100 m and 5%/°C (e.g., De Montety et al., 2018;  
221 Busenberg and Plummer, 1992).

222 The overall principle of CFC-SF<sub>6</sub> dating is that a given concentration of CFC-SF<sub>6</sub> in water,  
223 converted into atmospheric pressure (p<sub>atm</sub>) and associated to the atmospheric chronicle, provides an  
224 indication of the residence time. The CFC and SF<sub>6</sub> concentrations data for the northern hemisphere  
225 given by the software TRACER LPM (<https://www.usgs.gov/software/tracerlpm> – Jurgens et al., 2012)  
226 were used as an input parameter. The estimation of the residence time is linked to the conditions of  
227 infiltration in the soil and the water flow dynamics in the aquifer. A lumped parameter approach  
228 (Maloszewski and Zuber, 1982; Jurgens et al., 2012) can be used to compare the CFC and SF<sub>6</sub>  
229 measurements to the distribution of theoretical concentrations and thus correlate the  
230 measurements to the age of the groundwater in the system investigated. For the present study, we  
231 have used three classical models (Maloszewski and Zuber, 1982): the Piston flow model (PFM), the  
232 Exponential Mixing Model (EMM), and the Binary Mixing Model (BMM) represented in Fig. 3. The  
233 PFM model considers the system as a continuously flowing system in a tube where recent water  
234 compels older water (Fig. 3a). CFC data, in this case, leads to determination of “groundwater age.”  
235 The EMM corresponds to a vertical stratification of groundwater flow with a similar distribution of  
236 transit times, which increases logarithmically (Jurgens et al., 2012; Fig. 3b). The water sample is then  
237 an average of all the streamlines, and the obtained residence time corresponds to the “characteristic  
238 time,” which is in fact the mean of the residence time of all the streamlines. The BMM is a mixture of  
239 two components, which have evolved hydrologically independently and are mixed (Fig. 3c, d). We  
240 can thus provide one age for the two-components and a mixing proportion between these two  
241 components.

## 242 4. Results

### 243 4.1 Major element concentrations

244 Major element data for spring, piezometer, and borehole water analyzed for this study are  
245 presented in Supplementary Materials (SM Tables 2a, 2b; 3a, 3b; 4a, 4b).

246

#### 247 4.1.1 Spring and piezometer water

248 As apparent in Fig. 4, the data obtained from the springs sampled for this study from 2015–  
249 2018 are consistent with previously published data for the period 1986–2010. More importantly, our  
250 data suggests that piezometer water, when excluding the deepest waters, has geochemical  
251 characteristics very similar to those of spring water (Fig. 5, 6 and SM Fig 1 for the piper diagram).  
252 Both are marked by low conductivities, alkalinity, and pH values, ranging from 30–50  $\mu\text{S}/\text{cm}$ , 0.04 to  
253 0.44 meq/L, and 5.46 to 7.84, respectively. The Si concentrations vary from 3.7 ppm to 6.4 ppm for  
254 piezometer water and from 3.3 ppm to 5.1 ppm for spring water. The concentrations of major  
255 cations  $\text{Ca}^{2+}$ ,  $\text{Mg}^{2+}$ ,  $\text{Na}^+$ , and  $\text{K}^+$  in spring water range from 1.3 to 3.7 ppm, 0.3 to 0.9 ppm, 1.5 to 2.4  
256 ppm, and 0.2 to 1.1 ppm, respectively. For piezometer water, the concentrations range from 1.3 to  
257 4.0 ppm, 0.2 to 0.7 ppm, 1.7 to 3.1 ppm, and 0.5 to 1.5 ppm, respectively (Fig. 5). Slightly higher Si  
258 and  $\text{Na}^+$  concentrations in some Pz3 and Pz7 samples are, however, observed (Fig. 5d, e). The  $\text{NO}_3^-$   
259 and  $\text{SO}_4^{2-}$  concentrations of piezometer water are also close to those of spring water. Some of the  
260 deepest Pz3 and Pz5 samples can have much higher conductivities than the other piezometer  
261 samples (SM Table3a,b). For three different sampling periods, Pz3 deep water was analyzed in major  
262 elements. The data indicate that such water, in addition to being more conductive, has higher  
263 alkalinity and higher pH values than the other piezometer water as well as much higher major cations  
264 and anions concentrations (SM Table 3a).

## 265 4.1.2 Boreholes water

266 Compared to the spring and piezometer water, samples collected in the boreholes have  
267 higher pH, conductivities, and alkalinity values, with pH from 6.98 to 8.32, conductivity between 150  
268 and 270  $\mu\text{S}/\text{cm}$ , and alkalinity between 0,3 meq/L and 2,7 meq/L (Fig. 5a). Their concentrations in the  
269 main cations and anions are also different (Fig 5, Fig 6, SM Fig 1), with  $\text{Ca}^{2+}$  and  $\text{Mg}^{2+}$  concentrations  
270 four to eight times higher in deep water than in spring and piezometer water, and  $\text{Na}^+$  and  $\text{K}^+$   
271 concentrations up to one to four times higher. Si concentrations are more concentrated, usually by  
272 about twice the maximum.  $\text{NO}_3^-$  concentrations usually have lower values in deep borehole water  
273 with values close to zero in some of them (Fig. 6e). Finally,  $\text{Cl}^-$  and  $\text{SO}_4^{2-}$  concentrations for all groups  
274 of water (spring, piezometer, and deep borehole water) are in the same range of variations (Fig. 6).  
275 The data also show that the geochemical characteristics of the borehole water are quite different  
276 from one borehole to another and also within the same borehole.

## 277 - Borehole F5

278 The water column of borehole F5, when not perturbed for a long time and hence at a steady  
279 state of hydrological functioning, is divided into two conductivity zones, with a surface zone marked  
280 by low conductivity values closed to those observed in spring and piezometer water ( $\approx 30 \mu\text{S}/\text{cm}$ ) and  
281 a deeper zone of several 10 m thick characterized by high conductivity values ( $\approx 250 \mu\text{S}/\text{cm}$ ) (Fig. 7).  
282 The transition between the two zones is narrow and takes place over less than 1 m. Its depth  
283 depends on the sampling period: the higher the water level (i.e., high flow period in the catchment)  
284 the deeper the transition zone (Fig. 7). Geochemical data obtained on water samples collected in  
285 such hydrological steady-state boreholes point out that water sampled around 43 m deep has high  
286 concentrations in major cations,  $\text{HCO}_3^-$ , and Si, and low to zero concentrations in  $\text{NO}_3^-$  (Fig. 6). Water  
287 samples from 13–14 m deep during periods of high water, i.e., not in the vicinity of the conductivity  
288 transition zone (see Fig. 7), have much lower concentrations of major cations,  $\text{HCO}_3^-$ , Si, and higher  
289 concentrations of  $\text{NO}_3^-$ . This F5 surface water has the same geochemical characteristics as those of  
290 Pz5 water, located a few meters away from the F5 borehole, and defines the same range of

291 variability in all the binary diagrams studied (Fig. 5 and 6) and in the Piper diagrams (SM Fig. 1). The  
292 other samples, i.e., the 13 m deep water taken during the lower water period and thus in the vicinity  
293 near the conductivity transition zone in the water column (see Fig. 7), as well as the water sampled at  
294 23-27 m deep, define in all these diagrams (Fig. 5 and 6) an alignment between the above two water  
295 types.

296 In 2015, three pumping tests of a few hours, with the pump at the bottom of the borehole,  
297 were performed in borehole F5. As illustrated in Fig. 7b, the electrical conductivity profile of the  
298 water column was significantly modified, especially in its deeper part, with conductivity decreasing to  
299 50 to 90  $\mu\text{S}/\text{cm}$ , depending on the pumping dates. After the pumping, a slightly higher conductivity  
300 level around 21 m depth can be observed on some profiles (Fig. 7b). The data also highlights that the  
301 water column recovers its stationary profile with two contrasted conductivity zones in a few days  
302 (Fig. 7c). Several samples, collected along the water column a few hours after pumping or one or two  
303 days later when the profile was returning to equilibrium (Fig. 7 b, c), were analyzed in major  
304 elements. All these samples, including the samples collected at  $\approx 23$  m and  $\approx 45$  m, plot in Fig. 5 and 6  
305 along the linear trends defined between the unperturbed deep end-member and piezometer Pz5  
306 end-member.

#### 307 - Boreholes F6-F7-F8

308 The concentrations of major elements in F6, F7, and F8 boreholes, located on the northern  
309 slope, show that the deep water of the different boreholes has geochemical characteristics specific  
310 to each of them and different from those of borehole F5 (Fig. 5, 6). Deep water from the F6 borehole  
311 has relatively stable major element concentrations over time. This water has the highest  
312 conductivity, alkalinity,  $\text{Mg}^{2+}$ , and  $\text{Cl}^-$  concentrations of all the deep water sampled in the Strengbach  
313 catchment and the lowest Si and  $\text{Na}^+$  concentrations (Fig. 5). It has also high  $\text{Ca}^{2+}$  and  $\text{SO}_4^{2-}$   
314 concentrations, similar to those analyzed in F5 deep water, and as for this water, no  $\text{NO}_3^-$  (Fig. 6).  
315 Compared to borehole F6, the F7 and F8 deep water have lower alkalinity, conductivity,  $\text{Cl}^-$ ,  $\text{Ca}^{2+}$ , and  
316  $\text{Mg}^{2+}$  concentrations, but higher Si,  $\text{Na}^+$ , and  $\text{NO}_3^-$  concentrations, and similar  $\text{K}^+$  concentrations. F8

317 water has lower  $\text{Mg}^{2+}$ ,  $\text{Cl}^-$ , and  $\text{SO}_4^{2-}$  concentrations compared to F7 water. In addition, in the  $\text{SO}_4^{2-}$  vs.  
318  $\text{Mg}^{2+}$  (Fig. 6d) or vs.  $\text{Ca}^{2+}$  (Fig. 6c) concentrations diagrams, all deep water samples define a single  
319 linear and positive trend except for the F8 borehole, which plots in a different and negative trend.  
320 Compared to F6 and F5 deep water, the F7 and F8 deep water is marked by a higher range of  
321 variations in nearly all the major anion and cation concentrations, which, however, remain relatively  
322 small compared to the inter-borehole chemical variability described above.

323

#### 324 4.2 Sr, U, and Nd isotopic ratios

325 The  $^{87}\text{Sr}/^{86}\text{Sr}$  and  $^{143}\text{Nd}/^{144}\text{Nd}$  isotopic ratios and ( $^{234}\text{U}/^{238}\text{U}$ ) activity ratios are given in Table 1.  
326 The data indicate that spring water samples collected in this study display U-Sr isotopic systematics  
327 very similar to the one observed for water collected in 2004-2006 (Prunier 2008; Pierret et al., 2014)  
328 with similar ranges of  $^{87}\text{Sr}/^{86}\text{Sr}$  and ( $^{234}\text{U}/^{238}\text{U}$ ) variations for each studied spring (and similar  $^{87}\text{Sr}/^{86}\text{Sr}$   
329 ratio variations with discharge (Figures in supplementary material SM Fig. 2a,b). The data also  
330 confirm the existence of small but possibly significant variations of ( $^{234}\text{U}/^{238}\text{U}$ ) with discharge (Fig. SM  
331 Fig. 2b). The data also evidence similar  $^{87}\text{Sr}/^{86}\text{Sr}$  and ( $^{234}\text{U}/^{238}\text{U}$ ) ratios in piezometer and spring water  
332 (Fig. 8a,b) with  $^{87}\text{Sr}/^{86}\text{Sr}$  ratios between 0.72039 and 0.72627 in piezometer water and between  
333 0.72117 to 0.72785 in spring water, and with ( $^{234}\text{U}/^{238}\text{U}$ ) systematically  $< 1$  in spring and piezometer  
334 water except in one Pz7 sample, which has a ( $^{234}\text{U}/^{238}\text{U}$ ) ratio of  $1.168 \pm 0.003$  (Fig. 8b). Compared to  
335 spring and piezometer water, deep borehole water has much less radiogenic Sr ratios, ranging  
336 between 0.71416 (F5) to 0.71898 (F6), and have U activity ratios systematically  $> 1$  with values  
337 ranging between 1.071 and 1.103 in F7 and F8 borehole deep water, between 1.073 and 1.354 in F6  
338 borehole water, and around 2.000 in F5 borehole water (Table 1 and Fig. 8). For F5 borehole water,  
339 while deep water is isotopically not very variable over time, the Sr and U ratio of surface and  
340 intermediate water show much higher variability. Surface water collected during high water periods,  
341 far from the conductivity transition zone (see above), has values close to those of the piezometer  
342 Pz5. On the other hand, surface water taken during low flow, i.e., intermediate water and water after

343 a long pumping test, have more variable values intermediate between the values of Pz5 water and F5  
344 deep water. Compared to the variations of ( $^{87}\text{Sr}/^{86}\text{Sr}$ ) and ( $^{234}\text{U}/^{238}\text{U}$ ) ratios, the variations of  
345 ( $^{143}\text{Nd}/^{144}\text{Nd}$ ) ratios are much less important with similar values in surface and deep water, with  
346  $^{143}\text{Nd}/^{144}\text{Nd}$  values ranging from 0.51214 to 0.51227 in spring water, from 0.51220 to 0.51227 in  
347 piezometer water, and from 0.51219 (F8) to 0.51224 (F5), in borehole deep water (Table 1).

348

#### 349 **4.3 CFC and SF<sub>6</sub> data**

350 CFC and SF<sub>6</sub> data collected for this study are given in Table 2 with water concentrations given  
351 in pmol/L and atmospheric mixing concentrations in pptv. The data show that spring waters have  
352 high CFC concentrations: 155 to 272 pptv for CFC-11, 376 to 625 pptv for CFC-12, and 50 to 101 pptv  
353 for CFC-113. A few springs were also analyzed in 2006 and 2007 and data are given in Supplementary  
354 materials (SM Table 5). Are also given in supplementary materials the dissolved gas concentrations  
355 (Ne, Ar, N<sub>2</sub> and O<sub>2</sub>) (SM Table 6). The CFC concentrations obtained in 2006 and 2007 are very  
356 consistent with the values obtained 10 years later at a similar season (Fig. 9). As observed with the  
357 elementary and isotopic geochemical characteristics, the CFC and SF<sub>6</sub> concentrations in the  
358 piezometer water (Pz3, Pz5, and Pz7) are similar to those of springs (Fig. 9). For spring and  
359 piezometer water, the data show lower CFC concentrations during low flow periods (August 2015)  
360 than during high flow periods (May 2006, 2007, and 2015). The data may also indicate a decrease of  
361 CFC concentration with the increase of Si concentration for spring water. This trend is less apparent  
362 when piezometer data are added (Fig. 10).

363 CFC data from boreholes lead to water typologies similar to those observed with elemental  
364 or isotopic geochemistry data. Surface water from F5 (13-15 m deep) plot within the same range of  
365 variation as spring and piezometer water (Fig. 9). For this water as for spring and piezometer water,  
366 CFC concentrations in samples collected during high flow periods (May 2015) are higher than during  
367 low flow periods (August 2015). F5 borehole water collected at 23-26 m has concentrations between  
368 F5 deep water and surface water concentrations (Pz5 and "surface" water from F5) (e.g., in Fig. 10b).

369 Deep water from boreholes F6, F7, F8, and F5 has lower concentrations than in spring and  
370 piezometer water, 16 to 124 pptv, 131 to 383 pptv, 12 to 48 pptv for CFC-11, CFC-12, and CFC-113,  
371 respectively. The distinction between surface and deep water, evidenced by the CFC concentrations,  
372 is clearly illustrated in the CFC-11 vs. CFC-113 or CFC-12 vs. CFC-113 binary diagrams (Fig. 9), despite  
373 the scattering of the data of each of these water types. Compared to CFC concentrations, SF<sub>6</sub>  
374 concentrations in Strengbach water do not show a systematic difference between spring/piezometer  
375 water and deep water. Only the amplitude of the variation range is different, with concentrations  
376 ranging from 6 to 24 pptv in spring and piezometer water and from 2 to 50 pptv in borehole deep  
377 water. The highest SF<sub>6</sub> concentrations are analyzed in the deep water of borehole F5, with values far  
378 above the maximum values measured in the atmosphere (9 pptv in 2016). When these samples are  
379 not considered, the variation range in SF<sub>6</sub> concentrations is more limited ( $\approx$  2 - 15 pptv) and closer to  
380 that of surface water.

## 381 5. Discussion

382 Geochemical data, whether elementary concentrations,  $^{87}\text{Sr}/^{86}\text{Sr}$  and ( $^{234}\text{U}/^{238}\text{U}$ ) ratios, or tracer  
383 gases (CFC and SF<sub>6</sub>), show a systematic distinction between the values measured in spring and  
384 piezometer water, on the one hand, and in deep borehole water, on the other hand. These data also  
385 show second-order variability between the different piezometers and between the different deep  
386 water sampled in the boreholes.

### 387 5.1. Influence of borehole building materials on water chemistry

388 As detailed in section 2, boreholes and piezometers have been equipped with various  
389 materials (SM Table 1 in Supplementary Materials), which can potentially impact the chemical  
390 composition of waters. The major and trace element concentrations of these different materials  
391 were analyzed and leaching was carried out on each of them for additional analysis. The protocol is  
392 presented in the Supplementary Materials 3 (leaching experiments), with the related table of results  
393 (Table SM3) and Figures (Fig. SM3a, b). The plot of the data in (Fig. SM 3a, b) clearly show that the

394 trends defined in each of these diagrams by deep borehole water (F5, F6, F7, and F8) cannot be  
395 explained by the contribution of a chemical flux with the characteristics of one of these materials or  
396 of their leachate into a surface-type water end-member. The trends defined by the data points in the  
397 diagrams never go towards one of such potential end-members. Similarly, the trends defined in Fig.  
398 SM 3a, b by the piezometer data points are very similar to those defined by the spring water and do  
399 not show any specific bias towards one of possible pollution end-members, except for the deep  
400 water of piezometer pz3. The latter water samples in Fig SM 3 define linear trends from the more  
401 surface waters of the piezometer to the domain defined by the leachates of the soda-lime glass  
402 beads used as filters in the piezometers. Based on such observations, it can be suspected that at the  
403 bottom of the pz3 piezometer, the bead filter has construction defects, which causes leaching of  
404 these beads and hence pollution of the deep pz3 waters. For this reason, the deep piezometer water  
405 samples are no longer discussed in the following sections.

## 406 5.2 Hydrological Implications from geochemical characteristics of spring and piezometer waters

407 As shown in the result section, the geochemical characteristics of spring water collected  
408 between 2015 and 2018 are consistent with those collected and analyzed over the 1986–2010  
409 period, indicating similar hydrogeochemical contexts and processes at the origin of the geochemical  
410 signatures of spring water over these different periods. Hydrogeochemical modeling of the  
411 Strengbach spring water for the period 1986–2010 (Ackerer et al, 2018, 2020a) has made it possible  
412 (a) to better specify the nature of the water-rock interactions controlling the geochemical budget of  
413 this water, (b) to specify the origin of the chemostatic behavior of these sources (Ackerer et al., 2018,  
414 2020a), and (c) to explain the decoupling that exists between the time evolution of the Si-Na  
415 concentrations and Ca-K concentrations in the Strengbach spring water over the past 30 years  
416 (Ackerer et al., 2018). Furthermore, the simulation results show that the rock interacting with the  
417 water feeding these springs is neither a fresh granitic bedrock nor a surface saprolite type rock but an  
418 already slightly weathered granite corresponding to fractured saprolite rocks located between one to

419 a few meters deep (Ackerer et al., 2018). This conclusion is not specific to the Strengbach case. It is  
420 also proposed for a neighboring granitic catchment, the Ringelbach catchment, based on the  
421 modeling of the geochemical composition of the Ringelbach spring water (Lucas et al., 2017;  
422 Schaffhauser et al., 2014). Such conclusions are consistent with the hydrological schemes deduced  
423 for the Strengbach catchment from hydrologic modellings, i.e., water circulating in a shallow  
424 subsurface aquifer constituted by the relatively thin ( $< \approx 10$  m) porous saprolite above the more  
425 compact bedrock (Ackerer et al., 2020a; Weill et al., 2019). Furthermore, as previously proposed  
426 (Riotte and Chabaux, 1999; Pierret et al., 2014; Prunier et al., 2015), water interactions with already  
427 weathered granites readily explain the occurrence of  $(^{234}\text{U}/^{238}\text{U}) < 1$  in the stream and spring  
428 Strengbach water, including the spring water retained in the present study. Such an interpretation is  
429 consistent with  $^{234}\text{U}/^{238}\text{U} < 1$  measured in soil horizons of the Strengbach catchment (Prunier et al.,  
430 2015; Ackerer et al., 2016). The geochemical modeling studies also explain the different behavior of  
431 Ca and the Si-Na system in the Strengbach spring water, whether because of their different long-  
432 term concentration trends or the greater spatial variability of Ca concentrations compared to the Si  
433 ones (Ackerer et al., 2018, 2020a). Both are related to the different nature of the main minerals  
434 controlling the budget of these elements in the Strengbach spring water. Dissolution of albite is the  
435 main mineral source of Na in solution; biotite and feldspars are the main source of Si. The Ca in  
436 solution is essentially derived from the dissolution of apatite with a small contribution of anorthite  
437 (5–10% of the Ca). The predominant role of apatite or its alteration products on the Ca budget of the  
438 Strengbach surface water was also proposed from the Sr-Nd isotope ratios of the Strengbach surface  
439 water (Aubert et al., 2001; Stille et al., 2009). It is confirmed by the new Sr-Nd results obtained in the  
440 present study, which plot within the domain of previous Sr-Nd data between the apatite and  
441 plagioclase domains (Fig. 11). Incidentally, such a similitude shows that for the spring water, the  
442 alteration system controlling the Sr-Nd budget of water circulating in the regolith has not been  
443 significantly modified over the past 20 years at the difference of what is observed for soil solutions  
444 (Prunier et al., 2015; Schmitt et al. 2017; Chabaux et al., 2019 for more details on soil solutions).

445 Altogether, these data, acquired over the last 15 to 30 years in the Strengbach basin, lead to a fairly  
446 well-defined hydrogeochemical framework for the spring water of this basin, with a geochemical  
447 signature of the water acquired in a shallow subsurface aquifer formed by the more or less altered  
448 saprolite levels.

449 The observation that piezometer water has on average similar geochemical and isotopic  
450 characteristics to those of surface water, which are very different from deep water, indicates that  
451 such water in the Strengbach catchment circulates in a reservoir similar to that of spring water, i.e.,  
452 in porous fractured saprolite. This conclusion thus confirms the hypothesis made by Ackerer et al.  
453 (2020a) to model the geochemical composition of Strengbach piezometer waters.

454

### 455 5-3 Origin of the geochemical characteristics of deep borehole waters

#### 456 5-3-1 Water mixing processes

457 As seen in the Results section, the deep water collected in boreholes has geochemical and  
458 isotopic characteristics quite different from those of surface water. The data also show significant  
459 geochemical variation between and within wells. This is particularly visible in borehole F5, which is  
460 characterized by two contrasting water samples highlighting at least two inflows of water (Fig. 7a)  
461 with a surface water end-member having geochemical characteristics of spring/piezometer water  
462 and a deep water end-member marked by high conductivity values and geochemical characteristics  
463 relatively stable over time. The results also show that the other F5 water samples, i.e., those  
464 collected at 23-26 m, after a long pumping test, or in the vicinity of the conductivity transition zone,  
465 plot along a mixing line between the two end-members in classical binary elementary diagrams (Fig.  
466 5-6). The U, Sr, and Nd isotopic results, as well as CFC and SF6 data, confirm such a mixing  
467 interpretation as, for instance, all data of F5 water plots along mixing lines in the  $^{87}\text{Sr}/^{86}\text{Sr}$  vs  $1/\text{Sr}$   
468 diagram (Fig. 8a). The different mixing lines defined in this diagram are easily explained by the  
469 geochemical variations of the surface end-member over time, which are much more important than  
470 for the deep end-member. The anti-correlation defined by all F5 data points in the CFC-11 vs. SF6

471 diagram (Fig. 10c) can also be explained by the proposed mixing scenario with low SF6 content in  
472 surface and a deep water end-member concentrated in SF6. Altogether, these data evidence that in  
473 borehole F5, waters of intermediate depths, water taken after pumping, and water collected at the  
474 vicinity of the conductivity transition represent mixing in variable proportions between surface and  
475 deep water end-members, which is potentially induced by the pumping protocols used in this study.

476         Compared to the deep water collected in borehole F5 or to the deep water in borehole F6,  
477 the waters collected in F7 at 42 m and 47 m and in F8 at 27 m are marked by relatively large  
478 geochemical variations in nearly all the major anion and cation concentrations (Fig. 5 and 6). As for  
479 intermediary waters of borehole F5, such variability could be a consequence of the water pumping  
480 procedure because in both boreholes F7 and F8 such pumping was performed in the vicinity of a level  
481 of conductivity change in the water column (in Ranchoux 2020). For borehole F7, the chemical  
482 variability of the samples at 47 m is higher than at 42 m, with chemical compositions approaching  
483 those of the 42 m water when the conductivity transition between the two zones is close to the 47 m  
484 depth. These variations could therefore be interpreted in terms of mixing in varying proportions of  
485 two distinct water supplies within the water column, one close to 42 m depth and another one to 47  
486 m depth, implying that our sampling protocol allows a better sampling of water at 42 m depth than  
487 at 47 m depth. Overall, these different results illustrate the difficulty of precisely sampling the  
488 diversity of deep water in boreholes with the sampling protocols, which can induce mixing artifacts  
489 between the different water incomes supplying the water column. However, such a protocol is  
490 sufficient to geochemically identify one to two specific deep water end-members per borehole, the  
491 geochemical composition of which is discussed later. These deep water end-members can be  
492 systematically associated to fractured areas in the two cores recovered during borehole F5 and F6  
493 drilling or in camera logging (Ranchoux, 2020). This certainly confirms a system of water circulation in  
494 the deep part of the substratum principally controlled by the fractures structuring it (Chabaux et al.,  
495 2017).

496         5-3-2 Mineralogical control

497 The different deep water identified in boreholes F5, F6, F7, and F8 have conductivities, alkalinities,  
498 and pH much higher than those in surface water. Such a characteristic, also seen for the Ringelbach  
499 catchment (Lucas et al., 2017; Schaffhauser et al., 2014), confirms a different hydrogeochemical  
500 context for the deep water compared to surface water. Each of these water samples has its own  
501 geochemical characteristics, which is consistent with the interpretation that deep water circulations  
502 in the Strengbach catchment are located along with different fractures, each of them having its own  
503 hydrophysical and mineralogical characteristics. Among the parameters that can be involved to  
504 explain the distinction between surface water and deep water and between the different deep water  
505 themselves, there is the nature of water-rock interactions (primary and secondary minerals)  
506 occurring along the water pathway.

507 Saturation tests were performed for all water types in the Strengbach catchment using the  
508 Hydrogeochemical KIRMAT code (Gérard et al., 1996), which was recently used to contribute to the  
509 understanding of different issues such as groundwater salinization (Lucas et al., 2010; M’Nassri et al.,  
510 2019), weathering processes (Lucas et al., 2017; Ackerer et al., 2018) and hydrothermal alteration  
511 (Ngo et al., 2016). The minerals tested are the granite minerals and granite alteration products (clay  
512 minerals, carbonates, Fe oxides) with the same characteristics as those used for Strengbach springs  
513 modeling (Ackerer et al., 2018; 2020a). Phosphate phases (apatite) recognized as mineral phases  
514 controlling the budget of Sr, Nd, and probably Ca of surface water, i.e., stream, springs, and soil  
515 solutions (Aubert et al., 2001, 2002; Prunier et al., 2015; Chabaux et al., 2019) have also been tested  
516 based on the P total concentrations as well as Ca sulfates. Based on major element characteristics,  
517 three piezometer water samples (pz3, pz5, and pz7) and four borehole water samples (F5 deep, F6,  
518 F7 42 m, and F8 27m) have been selected for the saturation test. Besides, an average spring water  
519 composition has been used for the saturation test. Data used for the calculation are given in Table 3  
520 and the results of the saturation index are given in Table 4 and illustrated in Fig. 12.

521 The results confirm different water-rock interaction characteristics between surface  
522 (piezometer and spring water) and deep water from boreholes F5, F6, F7, and F8. In terms of primary

523 silicate minerals, the surface water is undersaturated in biotite and plagioclases (Ca and Na) and  
524 slightly in K-feldspars. They are also oversaturated in muscovite and quartz. Deep water is  
525 undersaturated in plagioclases only (especially Ca and slightly or not in Na plagioclases) and  
526 saturated in K-feldspars, muscovite, quartz, and most often in biotite. The differences between the  
527 two types of water signature are also found in secondary or minor minerals: surface and deep water  
528 are both saturated with kaolinite and illite, while only deep water is saturated with a  
529 montmorillonite-type clay mineral. Moreover, surface water is highly undersaturated with calcite or  
530 dolomite while deep water is undersaturated in dolomite and only slightly in calcite. These results  
531 highlight the very different saturation degree between these two types of water, confirming that  
532 surface water is mostly in a context of dissolution, involving a wide range of primary silicate minerals  
533 but also minor minerals such as apatite, and secondary minerals such as clay minerals (Ackerer et al.,  
534 2018, 2020a). The deep water is, by contrast, in a context of dissolution limited essentially to  
535 plagioclase and carbonates.

536 The observation that, in the  $^{143}\text{Nd}/^{144}\text{Nd}$  vs.  $^{87}\text{Sr}/^{86}\text{Sr}$  isotopic diagram (Fig. 11), spring and  
537 piezometer water is placed on or near the theoretical apatite-plagioclase mixing curve is consistent  
538 with the interpretation that in the Strengbach catchment, the surface water has a Sr-Nd budget  
539 controlled by the dissolution of these two minerals without significant Sr-Nd fractionation (Aubert et  
540 al., 2001). The offset of surface water with such a theoretical mixing curve has been proposed due to  
541 a contribution from a component of the atmospheric deposition type (Aubert et al., 2002). Compared  
542 to spring and piezometer water, borehole water is characterized by less radiogenic Sr isotope ratios.  
543 In the Sr-Nd isotopic diagram, the borehole water data thus defines a domain distinct from that of  
544 surface water (Fig. 11). Explaining the difference between the Sr-Nd systematic in surface and deep  
545 waters by a different atmospheric contribution in the two water types would imply a higher  
546 atmospheric contribution in the deep borehole water than in spring or piezometer water, which is  
547 difficult to consider. Thus, the deep-water data points in the Sr-Nd diagram, assuming for surface  
548 water a Sr-Nd budget essentially controlled by the phosphate-plagioclase minerals, would impose a

549 dissolution of these two minerals with a significant Sr-Nd fractionation at the difference of what we  
550 propose for surface water. An alternative explanation would be that the Sr and Nd chemical budget  
551 in deep water is controlled by an additional mineral phase and not only by the apatite plagioclase  
552 dissolution. Saturation tests indicate that deep water, in addition to being undersaturated in  
553 plagioclase, is also relatively undersaturated in carbonates. Carbonates are also observed as fracture  
554 minerals in cores (Ranchoux, 2020). We propose, therefore, that they can contribute to the Sr-Nd  
555 budget of deep water. Besides, if apatite dissolution in deep water-rock interaction is assumed not to  
556 fractionate Sr-Nd, as for surface water, the Sr and Nd isotope ratios of carbonates must have  
557 unradiogenic Sr and Nd to account for the deep water points in the Nd vs. Sr isotope ratio diagram.  
558 Observation of sulfate-rich water for boreholes F5, F6, and F7, and less rich for borehole F8, may also  
559 suggest a contribution of sulfate minerals in deep water-rock interactions in the Strengbach  
560 catchment. Sulfate minerals are observed in fractures (Lerouge pers. comm.), and their role is also  
561 invoked to explain some specific chemical characteristics of soil solutions (Prunier et al., 2015;  
562 Chabaux et al., 2019).

563 We, therefore, propose from the above geochemical and isotopic data that differences  
564 between surface and deep water in the Strengbach catchment are the consequence of two different  
565 water circulation contexts, with surface water circulating in a shallow subsurface aquifer or very  
566 fractured area and deep water circulating in a network of more or less independent fractures  
567 separated by fresh bedrock. The observation that borehole water at Strengbach has  $^{234}\text{U}/^{238}\text{U}$  activity  
568 ratios systematically  $> 1$ , whereas surface water (spring and piezometer water) has activity ratios  $< 1$ ,  
569 supports this pattern of different alteration contexts for the two types of water. For deep water, a  
570  $^{234}\text{U}$ - $^{238}\text{U}$  fractionation is classically expected in a fresh bedrock alteration context, i.e., at  $^{234}\text{U}/^{238}\text{U}$   
571 equilibrium. However, this pattern needs to be confirmed by  $^{234}\text{U}$ - $^{238}\text{U}$  analysis of rocks and minerals  
572 in fractures, which is beyond the scope of this study. In the Ringelbach catchment, Lucas et al. (2017)  
573 proposed that the chemical differences between surface and deep water and between two deep  
574 water samples result from their different hydrodynamic characteristics, namely, from different water

575 velocity and/or residence times between the two systems with faster water flow for surface water  
576 than for deep water. The observation that in the Strengbach catchment the saturation index of deep  
577 water increases with decreasing altitude (Fig. 12) may support the assumption that the groundwater  
578 residence time potentially plays an important role in the geochemical diversity of the Strengbach  
579 water. The CFC analysis makes it possible to discuss this point for the Strengbach catchment.

580

## 581 5-4 Water age dating

582

### 583 5.4.1 SF<sub>6</sub> lithogenic production

584 As for the chemical and isotopic data, the CFC data indicate a systematic difference between  
585 surface and deep water, which is interpreted as two different water circulation systems for surface  
586 water and deep water. The data also define positive trends in binary CFC diagrams (Fig. 9a, c). By  
587 contrast, no global correlation is observed between CFC and SF<sub>6</sub>. In almost all water samples, SF<sub>6</sub>  
588 concentrations are higher than the maximum SF<sub>6</sub> atmospheric concentrations with values as high as  
589 five times the maximum atmospheric values. A lithogenic production of SF<sub>6</sub> is often invoked to  
590 explain such high concentrations. SF<sub>6</sub> terrigenous flux was proposed, for instance, in diagenetic fluids  
591 (Busenberg and Plummer, 2000), basalt, or granitic rocks (Kranz 1966; Harnisch and Eisenhauer,  
592 1998; Busenberg and Plummer, 2000; Koh et al., 2007). SF<sub>6</sub> lithogenic production requires a fluor  
593 source in rocks, which can be found in some minerals such as magmatic micas, fluorapatites or  
594 fluorites. It also requires an energy source, which is often assumed to be linked to energy produced  
595 by  $\alpha$  decays of the U and Th series (Kranz, 1966). Fluorites or fluorapatites are observed in Vosges  
596 granites or fracture systems of the Vosges granites (Blanalt et al., 1972; Turpault et al., 1998).  
597 Occurrences of such minerals may thus provide a terrigenous SF<sub>6</sub> source in the Strengbach  
598 catchment, which prevents the use of SF<sub>6</sub> concentrations for water age estimation.

## 599 5.4.2 Age dating of spring and piezometer water

600 CFC data show similar values for spring and piezometer water consistent with the  
601 interpretation that these two water types circulate in a similar hydrological environment. The CFC  
602 values are relatively close to the current atmospheric values, both for the 2015–2018 or 2006–2007  
603 data. This implies young ages for this water. The dispersion of the CFC data is relatively high (Fig. 9),  
604 much higher than the analytical uncertainty. The dispersion of data in the CFC binary diagrams is  
605 classical and has been explained by different processes, which, in addition to the possible variation of  
606 recharge  $T^\circ$ , can be due to local atmospheric pollution leaks from landfills or agriculture (e.g., Oster  
607 et al., 1996; Ho et al., 1998; Hohener et al., 2003; Plummer et al., 2000; Spurlock et al., 2000;  
608 International Atomic Energy Agency, 2006; Darling et al., 2012) or to CFC microbial degradation in  
609 reductive context. Such microbial degradation affects CFC-11 much more than CFC-113 and, finally,  
610 CFC-12 (e.g., Cook et al., 1995; Plummer et al., 1998; Sebol et al., 2007; Horneman et al., 2008). In  
611 the Strengbach deep water, the correlation observed between CFC-11 and  $\text{NO}_3^-$  concentrations (Fig.  
612 10b), associated with low values of dissolved oxygen (Table SMT1), likely indicates the occurrence of  
613 CFC microbial degradation. CFC microbial degradation does not occur in an oxidizing environment  
614 and thus cannot be invoked for CFC scattering of surface water.

615 The observation that the spring and piezometric water collected in August 2015 during  
616 periods of low flow have systematically lower values than water from periods of higher flow might  
617 indicate mean residence times of water greater during low flow periods than during high flow  
618 periods with a potential difference of several years. Such age might even be consistent with the  
619 preliminary estimate of surface water residence time made in the Strengbach catchment from  
620 oxygen isotopic data (Viville et al., 2006). The global anticorrelation observed between the CFC-113  
621 concentrations and Si concentrations (Fig. 10a) might also reinforce such an interpretation if the Si  
622 concentrations of water were considered as a proxy of the water residence time within the aquifer  
623 (e.g., Marçais et al., 2018). However, a variation of water temperature recharge of  $\approx 1^\circ\text{C}$  can entirely

624 account for the CFC concentration range of the spring and piezometer water. The noble gases  
625 concentrations vary following a similar trend as CFC, with higher concentrations in high flow (May)  
626 and lower in low flow (August) periods (SM Table 6 in Supplementary Material). Such variations can  
627 result from a variation of the equilibration temperature of these dissolved gases at the season scale  
628 in the context of a monthly circulation of the surface water in the Strengbach catchment. The  
629 hydrological modeling works, using the NIHM code (Pan et al., 2015; Weill et al., 2019) as well as the  
630 coupled hydrogeochemical NIHM-KIRMAT modeling (Ackerer et al., 2020a), evidence short water  
631 transfer times of a few months maximum for the spring and piezometer water in the Strengbach  
632 catchment, which is not very variable from one hydrological period to another. The  
633 hydrogeochemical modeling exercise also explains the origin of the  $\text{SiO}_2$  concentration variations  
634 within the Strengbach surface water (Ackerer et al., 2020a). A seasonal variation of recharge  
635 temperature of the surface water in the Strengbach catchment is certainly the main cause of the  
636 observed CFC data dispersion. This implies that in such mid-mountain and headwater catchments  
637 where surface water circulates relatively quickly, the classical assumption of a constant recharge  
638 temperature to recalculate atmospheric concentrations of CFC is not applicable. The consequence is  
639 that in such a hydrogeological context, without an independent estimate of water recharge  
640 temperature, CFC can only be used as tracers of short residence time (less than a year to a few years)  
641 and cannot be used to infer more precise water ages.

#### 642 5.4.3 Age dating of borehole deep water

643 As seen in section 4.4, deep water has lower CFC concentrations than surface water and the  
644 data define a linear trend in the CFC-12 vs. CFC-113 diagram (Fig. 9b). In this diagram, the data does  
645 not plot along the theoretical curve given by the Piston Flow (PF) Model but rather along the  
646 theoretical curves from Binary Mixing (BM) Model and Exponential Mixing (EM) Model. These  
647 observations imply that the CFC data of the Strengbach borehole water cannot be interpreted with

648 the PF model but rather with the other two. The CFC data alone do not allow one model to be  
649 favored over the other. Therefore, they are discussed for both models.

650 In the case of the EM model, the CFC data mean that the groundwater residence time is  
651 greater than 30 years for F6 water (Table 2) and up to 130 years in the case of the less concentrated  
652 water (F5 and F8 in Tables 2). If we consider vertical circulation, the water's apparent velocity varies  
653 between 0.18 and 2.03 m/yr (Table 5), which is the order of magnitude typically used in modeling  
654 this type of circulation (e.g., Lucas et al., 2017). If we consider circulation in a fracture network, then  
655 the distance can increase considerably, inducing higher velocity. For a maximal distance proposed as  
656 the distance from the top added to the sampling depth (considering no tortuosity), the velocity  
657 obtained would vary between 1.56 and 11,97 m/yr (Table 5).

658 In the case of the BMM model with a straight line between the recent water and a point  
659 without CFC, i.e., before 1940, the deep-water concentration would be due to a mixture between  
660 recent water and water older than 80 years. The estimation of the proportion of recent and deep  
661 water can be calculated with a CFC-12 concentration to provide information on flow dynamics,  
662 considering a PF Model for recent water from 2018 to  $\approx$ 1995 and old water without CFC for the  
663 second end-member. The average values of the proportion of recent water obtained for each  
664 borehole are presented in Table 2. The proportion of recent water on deep water ranges from 70%  
665 to 27%, depending on the observed borehole and the sampling period. Similar values are obtained  
666 using O<sub>2</sub> values (Table 2) with values ranging from 60% to almost 0%. A relationship appears between  
667 the proportion of recent water and the location of the borehole along the watershed slope: when the  
668 borehole is located lower in the slope, the influence of recent water is lower. It is also observed that  
669 when the sampling is deeper in the borehole, the proportion of young water is lower. The  
670 comparison of data from a borehole with the nearby piezometer validates the mixing hypothesis. For  
671 the two pairs F5-Pz5 and F7-Pz7, in almost all cases for the same sampling period, the couple of

672 surface-deep samples aligns between a young/present day water component and a water end-  
673 member without CFC in the diagram CFC-12 vs. CFC-113.

674 In a context other than that of the Strengbach catchment, old deep saline fluids of several  
675 hundred thousand years have been observed at a few hundred meters deep in the fracture granitic  
676 basement (e.g., Bucher and Stober, 2010). Even not considering such depths, in the fracture granitic  
677 basement in Brittany, France, ancient water has also been seen at depths of  $\approx 100$  to 200 m (Roques  
678 et al., 2014a, b). These waters circulate slowly in circulation loops which can exceed the limits of  
679 surface watersheds. They can show mixing processes with surface water during high flow periods  
680 similar to those observed in the deep drillings of Strengbach (Roques et al., 2014a, b; Bochet et al.,  
681 2019). Within such systems, the slow deep circulation allows for partial equilibration of the water  
682 with the granitic matrix (micro-fracturation), which provides solutes with much higher residence  
683 times related to diffusion through the matrix (Aquilina et al., 2015; Aquilina and Dreuzy, 2011). We  
684 propose that such a scenario could be invoked to explain the CFC systematic of the Strengbach deep  
685 water, i.e., the water flowing in fractures is a mixture between recent water circulating rapidly  
686 through fracture networks and old water ( $> 80$  yrs) flowing either in secondary fractures or in the  
687 granitic matrix.

## 688 **6. Conclusion**

689 This study presents the water geochemical characteristic of the Strengbach catchment at  
690 different depths to bring better constraints of the deep alteration process, which occurs in a small  
691 granitic catchment. For this purpose, spring water (i.e., water circulating in the first meter of a  
692 saprolite aquifer), water from piezometers (i.e., from 10 to 15 m deep), and deep water (from 50 to  
693 120 m-deep boreholes) were sampled and analyzed under different hydrological conditions (high,  
694 intermediate, and low flow).

695 Chemical data show contrasted characteristics between spring and piezometer water, on the  
696 one hand, and water sampled in front of the main fractured area, on the other. Deep water is  
697 characterized by concentrations of major elements generally higher than those of more superficial  
698 water. This, therefore, highlights the existence of at least two types of water with contrasting  
699 signatures. Analysis of major elements as well as Sr and Nd isotopes shows that all the geochemical  
700 and isotopic signatures of the water of the catchment can be explained at first order by the primary  
701 mineralogy of the granite in place, and in particular by the dissolution of the phosphate-plagioclase  
702 minerals. Besides, the saturation index shows that chemical variations in water can be explained by a  
703 more advanced degree of alteration of primary minerals for deep water where minerals such as  
704 albite, anorthite, or biotite are closer to equilibrium.

705 CFC data show that the two types of water have very different ages. CFC concentration in  
706 surface water indicates recent ages. The data also suggests that the variations of CFC concentrations  
707 in spring and piezometer water, between the periods of high and low water, can result from a  
708 seasonal variation of recharge temperature of surface water. Such an interpretation implies that in a  
709 hydrological context of rapid surface water circulation, as in the Strengbach catchment, without an  
710 independent estimate of water recharge temperature, CFC data can mainly be used as tracers of  
711 short residence time (less than a year to a few years) without being able to determine the water ages  
712 more precisely. For deep water, the low CFC concentrations can be explained by (1) water with ages  
713 between 50 to 200 years or (2) a mixing between recent water having high concentrations of CFC and  
714 older than 70 years water without CFC, depending on the interpretation of the CFC mode used.  
715 Relationships between the deep boreholes and piezometers at intermediate depth observed for CFC  
716 as well as oxygen might favor the mixing interpretation as already observed in other fractured  
717 systems.

718 **Acknowledgment:** This work benefited from fruitful discussions with V. Vergnaud, E. Chatton, G.  
719 Schaefer, A. D. Schmitt, S. Rihs, and colleagues from the CANTARE ANR Program, i.e., F. Gal, C.

720 Dezayes, C. Lerouge, and P. Négrel. The study was financially supported by a Ph. D. scholarship  
721 awarded to C. Ranchoux by the University of Strasbourg, France. It was also supported by the French  
722 ANR Program under grant agreement ANR-15-CE06-0014 (Project CANTARE- Alsace). The drilling and  
723 equipment of the Strengbach boreholes were funded mainly by the CPER Alsace REALISE program  
724 (2007–2014) with a financial contribution of the ANR CRITEX project, one of the 2012–2020 French  
725 “Investment for Future” programs. The authors thank the Executive Editor Zimeng Wang, the AE  
726 Romain Millot, and two anonymous reviewers for their very constructive comments, which helped us  
727 to significantly improve the manuscript.

728

729 **Table captions**

730

731 **Table 1:** Isotopic  $^{87}\text{Sr}/^{86}\text{Sr}$  and  $^{143}\text{Nd}/^{144}\text{Nd}$  ratios, ( $^{234}\text{U}/^{238}\text{U}$ ) activity, and Sr, Nd, and U concentrations  
732 of boreholes, piezometers, and spring waters.

733

734 **Table 2:** CFC-SF<sub>6</sub> gas concentration in water (pmol/l), corresponding atmospheric mixing ratio (pptv),  
735 and simulation results of the PFM mean age, EMM mean age, and mix fraction of the young  
736 component of the BMM using CFC-12 values and TracerLPM software.737 **Table 3:** Average water concentrations of springs, piezometers, and boreholes used for the index  
738 saturation test.739 **Table 4:** Saturation Index of main minerals for the different water signatures. Negative values are  
740 highlighted in grey.741 **Table 5:** Minimum water velocity estimates based on sampling depths and residence time from the  
742 EMM model.

743

744 **Figure captions**

745

746 **Figure 1:** (a) and (b) localization and presentation of the Strengbach catchment with the position of  
747 springs (dark blue), piezometers (light blue), and deep boreholes (orange) in the basin; (b) and (c)  
748 simplified slope cross-sections with borehole localization.

749

750 **Figure 2:** Precipitation (dark histogram on top), stream discharge (light blue), and F5 borehole  
751 piezometric level (red line) from 2015 to 2019. Borehole, piezometer, and spring water (dark point),  
752 and CFCs-SF<sub>6</sub> (yellow point) sampling periods are highlighted.

753

754 **Figure 3:** schematic lumped parameter model used for the CFC-SF<sub>6</sub> interpretation of this study, with  
755 (a) Piston Flow Model (PFM), (b) Exponential Mixing Model (EMM), (c) and (d) Binary Mixing Model  
756 (BMM).

757

758 **Figure 4:** Time evolution of Na<sup>+</sup>, K<sup>+</sup>, Ca<sup>2+</sup>, Mg<sup>2+</sup> and Si concentrations of spring water from 1990 to  
759 2016 (data: Ackerer et al., 2018, 2020a; this study)

760

761 **Figure 5:** Concentration plots of water samples: (a) conductivity vs. pH, (b) Ca<sup>2+</sup> vs. alkalinity, (c) Ca<sup>2+</sup>  
762 vs. Mg<sup>2+</sup>, (d) Si vs. Na<sup>+</sup>, and (e) K<sup>+</sup> vs. Na<sup>+</sup>.

763

764 **Figure 6:** Concentration plots of water samples: (a) Cl<sup>-</sup> vs. alkalinity, (b) Cl<sup>-</sup> vs. NPOC, (c) SO<sub>4</sub><sup>2-</sup> vs. Ca<sup>2+</sup>,  
765 (d) SO<sub>4</sub><sup>2-</sup> vs. Mg<sup>2+</sup>, and (e) SO<sub>4</sub><sup>2-</sup> vs. NO<sub>3</sub><sup>-</sup>.

766

767 **Figure 7:** Borehole F5 conductivity profile evolution influenced by long pumping: (a) before pumping,  
768 (b) after pumping (around 5 hr), (c) coming back to equilibrium, and (d) acoustic scanner of borehole  
769 walls. The fractured area is highlighted in grey.

770

771 **Figure 8:** (a)  $^{87}\text{Sr}/^{86}\text{Sr}$  isotopic ratio vs. 1/Sr (ppm) and (b) ( $^{234}\text{U}/^{238}\text{U}$ ) activity ratio vs. 1/U (ppm) of  
772 Strengbach water samples. As an example, mixing lines of borehole F5 are represented with a full

773 line corresponding to the May 2015 sampling period, dashed lines for December 2015, and dotted  
774 lines for November 2016.

775  
776 **Figure 9:** Plot of (a) CFC-11 vs. CFC-113, (b) CFC-12 vs. CFC-113, and (c) CFC-11 vs. SF<sub>6</sub> of spring,  
777 piezometer, and borehole water from the Strengbach catchment. Theoretical curve given by Piston  
778 Flow Model (PFM – Black curve), Exponential Mixing Model (EMM – Grey curve) and Binary Mixing  
779 Model (BMM – dotted line). Dates of recharge are indicated on the PFM curve as well as the mean  
780 residence times on the EMM. The BMM curves consider a mixing between actual water (2018) and  
781 old groundwater (older than 80 years).

782  
783 **Figure 10:** Plot of (a) CFC-113 (pptv) vs. Si (mmol/l) of spring and piezometer water, and (b) CFC-11  
784 (pptv) vs. NO<sub>3</sub><sup>-</sup> (mmol/l) of boreholes and piezometer water.

785  
786 **Figure 11:** <sup>144</sup>Nd/<sup>143</sup>Nd vs. <sup>87</sup>Sr/<sup>86</sup>Sr diagram. Previously analyzed minerals (Aubert et al., 2001, 2002;  
787 Bosia pers. comm.) are represented. Several mixing hyperboles are also represented:

788 Yellow curve: Apatite-plagioclase mixing hyperbole using Sr and Nd concentrations and isotopic  
789 ratios measured in the two mineral end-members, namely, for apatite <sup>144</sup>Nd/<sup>143</sup>Nd = 0.5123, <sup>87</sup>Sr/<sup>86</sup>Sr  
790 = 0.7112, [Nd] = 430 ppm, and [Sr] = 752 ppm, and for plagioclase <sup>144</sup>Nd/<sup>143</sup>Nd = 0.5121, <sup>87</sup>Sr/<sup>86</sup>Sr =  
791 0.7365, [Nd] = 1 ppm, and [Sr] = 16 ppm. The percentages on the curve represent the contribution of  
792 apatite in apatite-plagioclase mixing.

793 Grey curve: Theoretical mixing hyperboles assuming a Nd-Sr fractionation during mineral dissolution.  
794 The full grey curve corresponds to a case with a very limited leaching of Nd from apatite ([Nd] = 4  
795 ppm instead of 430 ppm); the dotted grey line corresponds to a very small dissolution of Sr from  
796 plagioclase ([Sr] = 0.1 ppm instead of 16 ppm).

797 Dashed black curves: Mixing hyperboles between atmospheric end-member and a lithogenic  
798 weathering end-member resulting from dissolution of a apatite-plagioclase mixing without Sr-Nd  
799 fractionation. Atmospheric end-member: <sup>144</sup>Nd/<sup>143</sup>Nd = 0.5121, <sup>87</sup>Sr/<sup>86</sup>Sr = 0.71096, [Nd] = 25 ppm,  
800 and [Sr] = 360 ppm.

801  
802 **Figure 12:** Saturation Index (SI) of (a) quartz, (b) albite, (c) feldspath, (d) Muscovite, (e) biotite, (f)  
803 montmorillonite, (g) dolomite, and (h) illites for average values of spring, piezometer, and deep  
804 borehole waters from the Strengbach catchment.

805  
806

807 **References**

- 808 Ackerer, J., Lucas, Y., Chabaux, F., & Clément, A. (2018). Hydrogeochemical modeling (KIRMAT) of  
809 surface water-rock interactions in elementary granitic catchments (Ringelbach and Strengbach,  
810 Vosges Mountains, France). In EGU General Assembly Conference Abstracts (Vol. 20, p. 9121)
- 811 Ackerer, J., Jeannot, B., Delay, F., Weill, S., Lucas, Y., Fritz, B., Viville, D. & Chabaux, F., (2020a).  
812 Crossing hydrological and geochemical modeling to understand the spatiotemporal variability of  
813 water chemistry in an elementary watershed (Strengbach, France). Hydrology and Earth System  
814 Sciences Discussions. 10.5194/hess-2018-609.
- 815 Ameli, A. A., Beven, K., Erlandsson, M., Creed, I. F., McDonnell, J. J., & Bishop, K. (2017). Primary  
816 weathering rates, water transit times, and concentration-discharge relations: A theoretical analysis  
817 for the critical zone. *Water Resources Research*, 53(1), 942-960.
- 818 Aquilina, L., & De Dreuzy, J. R. (2011). Relationship of present saline fluid with paleomigration of  
819 basinal brines at the basement/sediment interface (Southeast basin–France). *Applied  
820 geochemistry*, 26(12), 1933-1945.
- 821 Aquilina, L., Vergnaud-Ayraud, V., Les Landes, A. A., Pauwels, H., Davy, P., Pételet-Giraud, E.,  
822 Labasque, T., Roques, C., Chatton, E., Bour, O., Ben Maamar, S., Dufresne, A., Khaska, M., Le Gal La  
823 Salle, C. & Barbécot, F. (2015). Impact of climate changes during the last 5 million years on  
824 groundwater in basement aquifers. *Scientific reports*, 5(1), 1-12.
- 825 Aubert, D., Stille, P., & Probst, A. (2001). REE fractionation during granite weathering and removal by  
826 waters and suspended loads: Sr and Nd isotopic evidence. *Geochimica et Cosmochimica Acta*, 65(3),  
827 387-406.
- 828 Aubert, D., Probst, A., Stille, P., & Viville, D. (2002). Evidence of hydrological control of Sr behavior in  
829 stream water (Strengbach catchment, Vosges Mountains, France). *Applied Geochemistry*, 17(3), 285-  
830 300.
- 831 Ayraud, V., Aquilina, L., Labasque, T., Pauwels, H., Molenat, J., Pierson-Wickmann, A. C., Durand, V.,  
832 Bour, O., Tarits, C., Le Corre, P., Fourre, E. Merot & P., Davy, P. (2008). Compartmentalization of  
833 physical and chemical properties in hard-rock aquifers deduced from chemical and groundwater age  
834 analyses. *Applied geochemistry*, 23(9), 2686-2707.
- 835 Azaël, S., 1990. Analyse structurale de quelques peuplements forestiers du bassin versant du  
836 Strengbach à Aubure (Haut-Rhin). Mémoire de DEA, Université Louis Pasteur, CEREG/UPL,  
837 Strasbourg.
- 838 Blanalt J.-G., Vogt H., Maire G. (1972). Carte géologique de la France au 1/50 000e, Brumath-  
839 Drusenheim [carte géologique], éch. 1/50 000e, Orléans, BRGM.
- 840 Bochet, O., Bethencourt, L., Dufresne, A., Farasin, J., Pédrot, M., Labasque, T., Chatton, E., Lavenant,  
841 N., Petton, C., Abbott, B.W., Aquilina, L. & Le Borgne, T. (2020). Iron-oxidizer hotspots formed by  
842 intermittent oxic–anoxic fluid mixing in fractured rocks. *Nature Geoscience*, 13(2), 149-155.
- 843 Bockgard, N., Rodhe A. & Olsson, KA. (2004). Accuracy of CFC groundwater dating in a crystalline  
844 bedrock aquifer: Data from a site in southern Sweden. *Hydrogeology Journal* 12(2): 171-183.

- 845 Brantley, S. L., Holleran, M. E., Jin, L., & Bazilevskaya, E. (2013). Probing deep weathering in the Shale  
846 Hills Critical Zone Observatory, Pennsylvania (USA): the hypothesis of nested chemical reaction fronts  
847 in the subsurface. *Earth Surface Processes and Landforms*, 38(11), 1280-1298.
- 848 Brantley, S. L., Lebedeva, M. I., Balashov, V. N., Singha, K., Sullivan, P. L., & Stinchcomb, G. (2017).  
849 Toward a conceptual model relating chemical reaction fronts to water flow paths in hills.  
850 *Geomorphology*, 277, 100-117.
- 851 Bu, X., Warner, M.J., 1995. Solubility of chlorofluorocarbon 113 in water and seawater. *Deep-Sea*  
852 *Res.* 42, 1151–1161.
- 853 Bullister, J.L., Wisegarver, D.P., Menzia, F.A., 2002. The solubility of sulfur hexafluoride in water and  
854 seawater. *Deep-Sea Res. Part I* 49, 175–187.) ;
- 855 Bucher, K. and Stober (2010) I. Fluids in the upper continental crust. *Geofluids* 10, 241–253.
- 856 Busenberg, E., & Plummer, L. N. (1992). Use of chlorofluorocarbons (CCl<sub>3</sub>F and CCl<sub>2</sub>F<sub>2</sub>) as hydrologic  
857 tracers and age-dating tools: The alluvium and terrace system of central Oklahoma. *Water Resources*  
858 *Research*, 28(9), 2257-2283.
- 859 Busenberg, E., & Plummer, L. N. (2000). Dating young groundwater with sulfur hexafluoride: Natural  
860 and anthropogenic sources of sulfur hexafluoride. *Water Resources Research*, 36(10), 3011-3030.
- 861 Buss, H. L., Brantley, S. L., Scatena, F. N., Bazilevskaya, E. A., Blum, A., Schulz, M., ... & Cole, D. (2013).  
862 Probing the deep critical zone beneath the Luquillo Experimental Forest, Puerto Rico. *Earth Surface*  
863 *Processes and Landforms*, 38(10), 1170-1186.
- 864 Cao, F., Jaunat, J., Vergnaud-Ayraud, V., Devau, N., Labasque, T., Guillou, A., Guillaneuf, A., Hubert, J.,  
865 Aquilina, L. & Ollivier, P. (2020). Heterogeneous behaviour of unconfined Chalk aquifers infer from  
866 combination of groundwater residence time, hydrochemistry and hydrodynamic tools. *Journal of*  
867 *Hydrology*, 581, 124433.
- 868 Chabaux, F., Cohen, A. S., Onions, R. K., & Hein, J. R. (1995). <sup>238</sup>U-<sup>234</sup>U-<sup>230</sup>Th chronometry of Fe-  
869 Mn crusts: Growth processes and recovery of thorium isotopic ratios of seawater. *Geochimica et*  
870 *Cosmochimica Acta*, 59(3), 633-638.
- 871 Chabaux, F., Granet, M., Larque, P., Riotte, J., Skliarov, E. V., Skliarova, O. Alexeieva, L & Risacher, F.  
872 (2011). Geochemical and isotopic (Sr, U) variations of lake waters in the Ol'khon Region, Siberia,  
873 Russia: Origin and paleoenvironmental implications. *Comptes Rendus Geoscience*, 343(7), 462-470.
- 874 Chabaux, F., Blaes, E., Stille, P., di Chiara Roupert, R., Pelt, E., Dosseto, A., Ma, L., Buss, H., Brantley,  
875 S.L. (2013). Regolith formation rate from U-series nuclides: Implications from the study of a  
876 spheroidal weathering profile in the Rio Icacos watershed (Puerto Rico). *Geochimica et*  
877 *Cosmochimica Acta*, 100, 73-95
- 878 Chabaux, F., Viville, D., Lucas, Y., Ackerer, J., Ranchoux, C., Bosia, C., Pierret, M. C., Labasque, T,  
879 Aquilina, L., Wyns, R., Lerouge, C., Dezaye, C. & Négrel, P. (2017). Geochemical tracing and modeling  
880 of surface and deep water–rock interactions in elementary granitic watersheds (Strengbach and  
881 Ringelbach CZOs, France). *Acta Geochimica*, 36(3), 363-366.
- 882 Chabaux, C., Stille, P., Prunier, J., Gangloff, S., Lemarchand, D., Morvan, G., Négrel, J., Pelt, E., Pierret,  
883 M.-C., Rihs. S., Schmitt, A.-D., Trémolières, M., & Viville, D. (2019). Plant-Soil-water interactions:

- 884 implications from U-Th-Ra isotope analysis in soils, soil solutions and vegetation (Strengbach CZO,  
885 France). *Geochimica et Cosmochimica Acta*.
- 886 Chauvel, C., Bureau, S., & Poggi, C. (2011). Comprehensive chemical and isotopic analyses of basalt  
887 and sediment reference materials. *Geostandards and Geoanalytical Research*, 35(1), 125-143.
- 888 Cook, P. G., Solomon, D. K., Plummer, L. N., Busenberg, E., & Schiff, S. L. (1995). Chlorofluorocarbons  
889 as tracers of groundwater transport processes in a shallow, silty sand aquifer. *Water Resources*  
890 *Research*, 31(3), 425-434.
- 891 Cook, P. G., Solomon, D. K., Sanford, W. E., Busenberg, E., Plummer, L. N., & Poreda, R. J. (1996).  
892 Inferring shallow groundwater flow in saprolite and fractured rock using environmental  
893 tracers. *Water Resources Research*, 32(6), 1501-1509.
- 894 Cook, P. G., Love, A. J., Robinson, N. I., & Simmons, C. T. (2005). Groundwater ages in fractured rock  
895 aquifers. *Journal of Hydrology*, 308(1-4), 284-301.
- 896 Corcho Alvarado, J. A., Purtschert, R., Hinsby, K., Troldborg, L., Hofer, M., Kipfer, R., Aeschbach-  
897 Hertig, W., & Arno-Synal, H. (2005).  $^{36}\text{Cl}$  in modern groundwater dated by a multi-tracer approach  
898 ( $^3\text{H}/^3\text{He}$ ,  $\text{SF}_6$ , CFC-12 and  $^{85}\text{Kr}$ ): a case study in quaternary sand aquifers in the Odense Pilot River  
899 Basin, Denmark. *Applied geochemistry*, 20(3), 599-609.
- 900 Darling, W. G., Goody, D. C., MacDonald, A. M., & Morris, B. L. (2012). The practicalities of using CFC  
901 and  $\text{SF}_6$  for groundwater dating and tracing. *Applied Geochemistry*, 27(9), 1688-1697.
- 902 Durand, S., Chabaux, F., Rihs, S., Düringer, Ph., Elsass Ph. (2005). U isotope ratios as tracers of  
903 groundwater inputs into surface waters: Example of the Upper Rhine hydrosystem. *Chemical*  
904 *Geology*, 220, 1-19
- 905 De Montety, V., Aquilina, L., Labasque, T., Chatton, E., Fovet, O., Ruiz, L., Fourné, E. & De Dreuzy, J. R.  
906 (2018). Recharge processes and vertical transfer investigated through long-term monitoring of  
907 dissolved gases in shallow groundwater. *Journal of hydrology*, 560, 275-288.
- 908 El Gh'mari, A. (1995). Etude de la dynamique d'altération d'un granite soumis à des précipitations  
909 atmosphériques acides (Doctoral dissertation, Thèse Doct. Univ. Louis Pasteur, Strasbourg).
- 910 Fichter, J. (1997). Minéralogie quantitative et flux d'éléments minéraux libéré par altération des  
911 minéraux des sols dans deux écosystèmes sur granite (bassin versant du Strengbach, Vosges)  
912 (Doctoral dissertation, Nancy 1).
- 913 Fichter J., Turpault M.P., Dambrine E. & Ranger J. (1998a). Localization of base cations in particle size  
914 fractions of acid forest soils. *Geoderma* 82, 295-314.
- 915 Fichter J., Turpault M.P., Dambrine E. & Ranger J. (1998b). Mineral evolution in acid forest soils of the  
916 Strengbach catchment. *Geoderma* 82, 315-340.
- 917 Gangloff S., Stille P., Pierret M.-C., Weber T. & Chabaux F. (2014). Characterization and evolution of  
918 dissolved organic matter in acidic forest soil and its impact on the mobility of major and trace  
919 elements (case of the Strengbach watershed). *Geochimica et Cosmochimica Acta*. 130, 21-41
- 920 Geagea, M. L., Stille, P., Millet, M., & Perrone, T. (2007). REE characteristics and Pb, Sr and Nd  
921 isotopic compositions of steel plant emissions. *Science of the Total Environment*, 373(1), 404-419.

- 922 Gerard, F., Clement, A., Fritz, B., & Crovisier, J. L. (1996). Introduction des phénomènes de transport  
923 dans le modèle thermo-cinétique KINDIS: le modèle KIRMAT. Comptes rendus de l'Académie des  
924 sciences. Série 2. Sciences de la terre et des planètes, 322(5), 377-384.
- 925 Gleeson, T., Befus, K. M., Jasechko, S., Luijendijk, E., & Cardenas, M. B. (2016). The global volume and  
926 distribution of modern groundwater. *Nature Geoscience*, 9(2), 161-167.
- 927 Guéguen, F., Stille, P., Geagea, M. L., & Boutin, R. (2012). Atmospheric pollution in an urban  
928 environment by tree bark biomonitoring—Part I: Trace element analysis. *Chemosphere*, 86(10), 1013-  
929 1019.
- 930 Hahm, W. J., Rempe, D. M., Dralle, D. N., Dawson, T. E., Lovill, S. M., Bryk, A. B., ... & Dietrich, W. E.  
931 (2019). Lithologically controlled subsurface critical zone thickness and water storage capacity  
932 determine regional plant community composition. *Water Resources Research*, 55(4), 3028-3055.
- 933 Harnisch, J., & Eisenhauer, A. (1998). Natural CF<sub>4</sub> and SF<sub>6</sub> on Earth. *Geophysical Research*  
934 *Letters*, 25(13), 2401-2404.
- 935 Heaton, T. H. E., & Vogel, J. C. (1981). "Excess air" in groundwater. *Journal of Hydrology*, 50, 201-216.
- 936 Ho, D. T., Schlosser, P., Smethie, W. M., & Simpson, H. J. (1998). Variability in atmospheric  
937 chlorofluorocarbons (CCl<sub>3</sub>F and CCl<sub>2</sub>F<sub>2</sub>) near a large urban area: Implications for groundwater  
938 dating. *Environmental science & technology*, 32(16), 2377-2382.
- 939 Höhener, P., Werner, D., Balsiger, C., & Pasteris, G. (2003). Worldwide occurrence and fate of  
940 chlorofluorocarbons in groundwater.
- 941 Holbrook, W. S., Marcon, V., Bacon, A. R., Brantley, S. L., Carr, B. J., Flinchum, B. A., Flinchum, B. A.,  
942 Richter, D.D., & Riebe, C. S. (2019). Links between physical and chemical weathering inferred from a  
943 65-m-deep borehole through Earth's critical zone. *Scientific reports*, 9(1), 4495.
- 944 Horneman, A., Stute, M., Schlosser, P., Smethie Jr, W., Santella, N., Ho, D. T., Mailloux, B., Gorman, E.,  
945 Zheng, Y. & Van Geen, A. (2008). Degradation rates of CFC-11, CFC-12 and CFC-113 in anoxic shallow  
946 aquifers of Araihasar, Bangladesh. *Journal of contaminant hydrology*, 97(1-2), 27-41.
- 947 International Atomic Energy Agency (2006). Use of chlorofluorocarbons in hydrology: a guidebook.  
948 Internat. Atomic Energy Agency.
- 949 Jankovec, J., Vitvar, T., Šanda, M., Matsumoto, T. & Han, L. F. (2017). Groundwater recharge and  
950 residence times evaluated by isotopes of hydrogen and oxygen, noble gases and CFCs in a mountain  
951 catchment in the Jizera Mts., northern Czech Republic. *Geochemical Journal*, 51(5), 423-437.
- 952 Jaunat, J., Huneau, F., Dupuy, A., Celle-Jeanton, H., Vergnaud-Ayraud, V., Aquilina, L., Labasque, T. &  
953 Le Coustumer, P. (2012). Hydrochemical data and groundwater dating to infer differential flowpaths  
954 through weathered profiles of a fractured aquifer. *Applied Geochemistry*, 27(10), 2053-2067.
- 955 Jurgens, Bryant & Bohlke, J. & Eberts, Sandra. (2012). TracerLPM (Version 1): An Excel® workbook for  
956 interpreting groundwater age distributions from environmental tracer data. U.S. Geol. Surv. Tech.  
957 Methods Rep.. 4-F3. 60. 10.3133/tm4F3.

- 958 Koh, D. C., Plummer, L. N., Busenberg, E., & Kim, Y. (2007). Evidence for terrigenous SF<sub>6</sub> in groundwater  
959 from basaltic aquifers, Jeju Island, Korea: Implications for groundwater dating. *Journal of*  
960 *Hydrology*, 339(1-2), 93-104
- 961 Kranz, R. (1966). Organische Fluor-Verbindungen in den Gaseinschlüssen der Wölsendorfer  
962 Flußspäte. *Naturwissenschaften*, 53(23), 593-600.
- 963 Labasque, T., Chaumery, C., Aminot, A., & Kergoat, G. (2004). Spectrophotometric Winkler  
964 determination of dissolved oxygen: re-examination of critical factors and reliability. *Marine*  
965 *Chemistry*, 88(1-2), 53-60.
- 966 Labasque, T. (2006). Analyse des CFC dans les eaux souterraines. Géosciences Rennes. Cahiers  
967 techniques de Géosciences Rennes, Rennes.
- 968 Labasque, T., Aquilina, L., Vergnaud, V., & Barbecot, F. (2014). Inter-laboratory comparison of the  
969 analyses of sulphur hexafluoride (SF<sub>6</sub>) and three chlorofluorocarbons (CFC-11,-12 and-113) in  
970 groundwater and an air standard. *Applied geochemistry*, 50, 118-129.
- 971 Ladouche, B., Probst, A., Viville, D., Idir, S., Baqué, D., Loubet, M., Probst, J.-L., & Bariac, T. (2001).  
972 Hydrograph separation using isotopic, chemical and hydrological approaches (Strengbach catchment,  
973 France). *Journal of hydrology*, 242(3-4), 255-274.
- 974 Liu, F., Conklin, M. H., & Shaw, G. D. (2017). Insights into hydrologic and hydrochemical processes  
975 based on concentration-discharge and end-member mixing analyses in the mid-Merced River Basin,  
976 Sierra Nevada, California. *Water Resources Research*, 53(1), 832-850.
- 977 Lucas, Y., Schmitt, A. D., Chabaux, F., Clément, A., Fritz, B., Elsass, P., & Durand, S. (2010).  
978 Geochemical tracing and hydrogeochemical modelling of water–rock interactions during salinization  
979 of alluvial groundwater (Upper Rhine Valley, France). *Applied Geochemistry*, 25(11), 1644-1663.
- 980 Lucas, Y., Chabaux, F., Schaffhauser, T., Fritz, B., Ambroise, B., Ackerer, J., & Clément, A. (2017).  
981 Hydrogeochemical modeling (KIRMAT) of spring and deep borehole water compositions in the small  
982 granitic Ringelbach catchment (Vosges Mountains, France). *Applied geochemistry*, 87, 1-21.
- 983 Małozzewski, P., & Zuber, A. (1982). Determining the turnover time of groundwater systems with the  
984 aid of environmental tracers: 1. Models and their applicability. *Journal of hydrology*, 57(3-4), 207-  
985 231.
- 986 Marçais, J., Gauvain, A., Labasque, T., Abbott, B. W., Pinay, G., Aquilina, L., Chabaux, F., Viville, D. &  
987 de Dreuzy, J. R. (2018). Dating groundwater with dissolved silica and CFC concentrations in crystalline  
988 aquifers. *Science of the Total Environment*, 636, 260-272.
- 989 M'Nassri, S., Lucas, Y., Schäfer, G., Dridi, L., & Majdoub, R. (2019). Coupled hydrogeochemical  
990 modelling using KIRMAT to assess water-rock interaction in a saline aquifer in central-eastern  
991 Tunisia. *Applied geochemistry*, 102, 229-242.
- 992 National Research Council (NRC). 2001. Basic Research Opportunities in Earth Science. The National  
993 Academies Press: Washington, DC.

- 994 Ngo, V. V., Lucas, Y., Clément, A., & Fritz, B. (2016). Modeling the impact of temperature on the  
995 saturation state and behavior of minerals in the Soultz-sous-Forêts geothermal  
996 system. *Geothermics*, 64, 196-208.
- 997 O'Geen, A., Safeeq, M., Wagenbrenner, J., Stacy, E., Hartsough, P., Devine, S., ... & Bales, R. (2018).  
998 Southern Sierra Critical Zone Observatory and Kings River Experimental Watersheds: A synthesis of  
999 measurements, new insights, and future directions. *Vadose Zone Journal*, 17(1), 1-18.
- 1000 Oster, H., C. Sonntag, et al. (1996). "Groundwater age dating with chlorofluorocarbons." *Water*  
1001 *Resources Research* 32(10): 2989-3001.
- 1002 Pan, Y., Weill, S., Ackerer, P. and Delay, F. (2015). A coupled stream flow and depth integrated  
1003 subsurface flow model for catchment hydrology, *Journal of Hydrology*, 530, 66\78.
- 1004 Pelt, E., Chabaux, F., Stille, P., Innocent, C., Ghaleb, B., Gérard, M., & Guntzer, F. (2013). Atmospheric  
1005 dust contribution to the budget of U-series nuclides in soils from the Mount Cameroon  
1006 volcano. *Chemical Geology*, 341, 147-157.
- 1007 Pierret, M.C., Stille, P., Prunier, J., Viville, D., & Chabaux, F. (2014). Chemical and U-Sr isotopic  
1008 variations in stream and source waters of the Strengbach watershed (Vosges mountains, France).  
1009 *Hydrology and Earth System Science*, 18(10), 3969-3985.
- 1010 Plummer, L. N., Busenberg, E., Drenkard, S., Schlosser, P., Ekwurzel, B., Weppernig, R., McConnell,  
1011 J.B. & Michel, R. L. (1998). Flow of river water into a karstic limestone aquifer—2. Dating the young  
1012 fraction in groundwater mixtures in the Upper Floridan aquifer near Valdosta, Georgia. *Applied*  
1013 *geochemistry*, 13(8), 1017-1043.
- 1014 Plummer, L. N., Rupert, M. G., Busenberg, E., & Schlosser, P. (2000). Age of irrigation water in ground  
1015 water from the Eastern Snake River Plain aquifer, south-central Idaho. *Groundwater*, 38(2), 264-283.
- 1016 Prunier, J., 2008. Etude du fonctionnement d'un écosystème forestier en climat tempéré, par l'apport  
1017 de la géochimie élémentaire et isotopique (Sr, U-Th-Ra): Cas du bassin versant du Strengbach  
1018 (Vosges, France) (Doctoral dissertation, Université Louis Pasteur (Strasbourg)).
- 1019 Prunier J., Chabaux F., Stille P., Pierret MC, Viville D., Gangloff S. (2015) Monitoring of geochemical  
1020 and isotopic (Sr,U) signatures in soil solutions for the evaluation of soil weathering evolution (the  
1021 Strengbach case) *Chemical Geology*, 417, 289–305.
- 1022 Ranchoux C. (2020). Caractérisation géochimique et datation des circulations d'eaux profondes dans  
1023 la zone critique : cas du Bassin versant du Strengbach. Doctoral dissertation in geochemistry under  
1024 the direction of F. Chabaux, Strasbourg, University of Strasbourg.
- 1025 Riebe, C. S., Hahm, W. J., Brantley, S. L. (2017). Controls on deep critical zone architecture: A  
1026 historical review and four testable hypotheses. *Earth Surface Processes and Landforms*, 42(1), 128-  
1027 156.
- 1028 Riotte J., Chabaux F. 1999. ( $^{234}\text{U}/^{238}\text{U}$ ) activity ratios in freshwaters as tracers of hydrological  
1029 processes: The Strengbach watershed (Vosges, France). *Geochim. Cosmochim. Acta*, 63, pp. 1263-  
1030 1275.

- 1031 Roques, C., Bour, O., Aquilina, L., Dewandel, B., Leray, S., Schroetter, J. M., Longuevergne, L., Le  
1032 Borgne, T., Hochreutener, R., Labasque, T., Lavenant, N., Vergnaud-Ayraud, V. & Mougin, B. (2014a).  
1033 Hydrological behavior of a deep sub-vertical fault in crystalline basement and relationships with  
1034 surrounding reservoirs. *Journal of Hydrology*, 509, 42-54.
- 1035 Roques, C., Aquilina, L., Bour, O., Maréchal, J. C., Dewandel, B., Pauwels, H., Labasque, T., Vergnaud-  
1036 Ayraud, V. & Hochreutener, R. (2014b). Groundwater sources and geochemical processes in a  
1037 crystalline fault aquifer. *Journal of hydrology*, 519, 3110-3128.
- 1038 Schaffhauser, T., Chabaux, F., Ambroise, B., Lucas, Y., Stille, P., Reuschlé, T., Perrone, T., & Fritz, B.  
1039 (2014). Geochemical and isotopic (U, Sr) tracing of water pathways in the granitic Ringelbach  
1040 catchment (Vosges Mountains, France). *Chemical Geology*, 374, 117-127
- 1041 Schmitt, A. D., Gangloff, S., Labolle, F., Chabaux, F., & Stille, P. (2017). Calcium biogeochemical cycle  
1042 at the beech tree-soil solution interface from the Strengbach CZO (NE France): insights from stable Ca  
1043 and radiogenic Sr isotopes. *Geochimica et Cosmochimica Acta*, 213, 91-109.
- 1044 Sebol, L. A., Robertson, W. D., Busenberg, E., Plummer, L. N., Ryan, M. C., & Schiff, S. L. (2007).  
1045 Evidence of CFC degradation in groundwater under pyrite-oxidizing conditions. *Journal of*  
1046 *Hydrology*, 347(1-2), 1-12.
- 1047 Spurlock, F., Burow, K. & Dubrovsky, N. (2000). "Chlorofluorocarbon dating of herbicide-containing  
1048 well waters in Fresno and Tulare counties, California." *Journal of Environmental Quality* 29(2): 474-  
1049 483.
- 1050 Stille P., Pierret M.C., Steinmann M., Chabaux F., Gauthier-Lafaye F., Pourcelot L., Viville D., Boutin R.  
1051 and Morvan G. (2009). Impact of atmospheric deposition, biogeochemical cycling and water–mineral  
1052 interaction on REE fractionation in acidic surface soils and soil water (the Strengbach case) *Chemical*  
1053 *Geology*, 264, 173-186
- 1054 Sugisaki, R., & Taki, K. (1987). Simplified analyses of He, Ne, and Ar dissolved in natural waters.  
1055 *Geochemical Journal*, 21(1), 23-27. Turpault, M. P., Bonnaud, P., & Dambrine, F. (1998). Dissolution  
1056 rate of fluor-apatite crystals inserted in acid soils of a forested catchment (Vosges Mountains, NE  
1057 France). *Mineralogical Magazine*, 62, 6.
- 1058 Tricca, A., Stille, P., Steinmann, M., Kiefel, B., Samuel, J., & Eikenberg, J. (1999). Rare earth elements  
1059 and Sr and Nd isotopic compositions of dissolved and suspended loads from small river systems in  
1060 the Vosges mountains (France), the river Rhine and groundwater. *Chemical Geology*, 160(1-2), 139-  
1061 158.
- 1062 Turpault, M. P., Bonnaud, P., & Dambrine, F. (1998). Dissolution rate of fluor-apatite crystals inserted  
1063 in acid soils of a forested catchment (Vosges Mountains, NE France). *Mineralogical Magazine*, 62, 6.
- 1064 Viville, D., Ladouche, B., & Bariac, T. (2006). Isotope hydrological study of mean transit time in the  
1065 granitic Strengbach catchment (Vosges massif, France): application of the FlowPC model with  
1066 modified input function. *Hydrological Processes: An International Journal*, 20(8), 1737-1751.
- 1067 Viville, D., Chabaux, F., Stille, P., Pierret, M.C., & Gangloff, S. (2012). Erosion and weathering fluxes in  
1068 granitic basins: the example of the Strengbach catchment (Vosges massif, eastern France). *Catena*,  
1069 92, 122-129.

- 1070 Warner, M.J. and Weiss, R.F., (1985). Solubilities of chlorofluorocarbons 11 and 12 in water and  
1071 seawater. *Deep-Sea Res.* 32, 1485–1497);
- 1072 Weill, S., Lesparre, N., Jeannot, B., & Delay, F. (2019). Variability of water transit time distributions at  
1073 the Strengbach catchment (Vosges Mountains, France) inferred through integrated hydrological  
1074 modeling and particle tracking algorithms. *Water*, 11(12), 2637.

Journal Pre-proof

Table 1:

Type	Name	Depth (m)	Date	Sr	Nd	U	$^{87}\text{Sr}/^{86}\text{Sr}$		$(^{234}\text{U}/^{238}\text{U})$		$^{143}\text{Nd}/^{144}\text{Nd}$			
							(2SE)	(2SE)	(2SE+0,5*10 <sup>-5</sup> )					
Borehole	F5	13	10/11/2015	70.90	0.006	22.50	0.714996	± 7	1.953	± 3	0.51223	± 3		
		14	12/11/2015	26.40	0.019	4.30	0.716876	± 9	1.728	± 1	-	± -		
		15	05/05/2015	13.10	0.026	0.22	0.722504	± 12	0.873	± 2	0.51226	± 3		
		15	26/08/2015	15.90	0.026	1.06	0.719441	± 11	1.364	± 2	0.51224	± 3		
		15	02/12/2015	8.70	0.029	0.26	0.724714	± 13	0.938	± 1	0.51226	± 3		
		15*	10/11/2015	19.30	0.022	3.03	0.718447	± 9	1.614	± 4	0.51224	± 3		
		23	23/11/2016	20.91	0.009	3.87	0.717270	± 7	1.758	± 2	0.51220	± 1		
		26	05/05/2015	20.90	0.024	2.04	0.718890	± 13	1.816	± 2	0.51226	± 3		
		26	26/08/2015	31.50	0.004	3.92	0.715910	± 10	1.805	± 2	-	± -		
		26	10/11/2015	120.00	<l.d	46.50	0.714096	± 7	1.983	± 4	-	± -		
		26	12/11/2015	43.00	0.004	8.56	0.715163	± 8	1.842	± 1	-	± -		
		26	02/12/2015	84.78	0.001	31.50	0.714258	± 6	1.982	± 1	-	± -		
		26*	10/11/2015	36.40	0.004	8.31	0.716311	± 8	1.680	± 2	0.51227	± 3		
		40	05/05/2015	121.00	0.004	52.30	0.714065	± 14	2.019	± 2	-	± -		
		40	26/08/2015	72.80	<l.d	23.10	0.714516	± 10	1.994	± 2	-	± -		
		40	10/11/2015	126.00	<l.d	47.90	0.713944	± 6	1.991	± 3	-	± -		
		40	12/11/2015	103.00	<l.d	37.90	0.714248	± 9	1.961	± 1	-	± -		
		40	02/12/2015	100.00	<l.d	38.80	0.714083	± 6	1.990	± 1	-	± -		
		40*	10/11/2015	34.70	0.006	7.87	0.716387	± 11	1.713	± 3	-	± -		
		43	23/11/2016	88.83	<l.d	33.20	0.714073	± 6	1.935	± 1	0.51222	± 4		
		48	10/11/2015	124.00	<l.d	47.70	0.714051	± 5	1.981	± 3	-	± -		
		48	12/11/2015	94.00	<l.d	36.00	0.714319	± 7	1.932	± 1	-	± -		
		48*	10/11/2015	38.20	0.006	9.21	0.716213	± 6	1.748	± 2	-	± -		
		49*	02/12/2015	15.14	0.008	1.49	0.718959	± 10	1.697	± 1	-	± -		
		F6	F6	63	27/10/2016	16.51	0.002	6.93	0.719292	± 7	1.354	± 1	-	± -
				63	22/11/2016	12.11	0.003	3.86	0.718662	± 6	1.073	± 1	0.51220	± 3
		F7	F7	45	26/08/2015	82.80	0.003	24.40	0.715566	± 7	1.071	± 1	-	± -
				46	26/10/2016	81.97	0.003	29.60	0.715583	± 7	1.090	± 1	-	± -

		42	22/11/2016	53.82	0.006	13.90	0.715593	± 8	1.079	± 1	0.51223	± 3
		47	22/11/2016	77.84	0.002	30.80	0.715588	± 7	1.099	± 1	0.51221	± 1
	F8	27	22/11/2016	114.00	0.005	79.90	0.715201	± 8	1.103	± 1	0.51219	± 2
		45	22/11/2016	110.00	0.002	87.60	0.715248	± 8	1.095	± 1	-	± -
<b>Piezometer</b>	Pz3	11	26/08/2015	7.96	0.074	0.53	0.724897	± 12	0.860	± 2	-	± -
		11	22/11/2016	5.88	0.101	0.69	0.724694	± 8	0.850	± 1	0.51227	± 1
		13	22/11/2016	20.99	0.007	0.73	0.720393	± 9	0.883	± 1	0.51220	± 1
	Pz5	13	23/11/2016	7.27	0.025	0.40	0.724958	± 8	0.897	± 1	0.51225	± 1
	Pz7	12	26/08/2015	9.90	0.133	1.06	0.726271	± 10	1.168	± 1	-	± -
		13	22/11/2016	8.09	0.099	1.15	0.724853	± 9	0.985	± 2	0.51220	± 2
<b>Spring</b>	ARG		05/05/2015	8.05	0.031	0.06	0.726939	± 9	0.929	± 4	0.51224	± 1
			26/08/2015	7.66	0.041	0.10	0.726212	± 12	0.910	± 5	0.51222	± 1
	CS1		05/05/2015	6.93	0.285	0.30	0.727848	± 3	0.881	± 2	0.51225	± 3
			26/08/2015	6.04	0.093	0.13	0.725587	± 9	0.868	± 2	0.51214	± 5
			10/11/2015	6.44	0.102	0.17	0.725475	± 6	0.872	± 1	-	± -
			02/12/2015	7.01	0.251	0.23	0.727235	± 7	0.877	± 2	-	± -
	CS2		05/05/2015	9.79	0.051	0.15	0.725390	± 7	0.877	± 1	0.51226	± 1
			26/08/2015	8.74	0.051	0.23	0.725260	± 9	0.874	± 2	0.51225	± 2
			10/11/2015	8.94	0.050	0.24	0.725265	± 3	0.877	± 1	-	± -
	CS3		05/05/2015	9.51	0.043	0.36	0.722197	± 6	0.829	± 1	0.51217	± 2
			26/08/2015	9.34	0.012	0.21	0.722333	± 10	0.824	± 1	0.51216	± 4
			10/11/2015	10.70	0.016	0.25	0.722138	± 7	0.825	± 1	-	± -
	CS4		05/05/2015	7.83	0.179	0.27	0.726496	± 10	0.882	± 1	0.51225	± 1
			26/08/2015	9.42	0.057	0.24	0.723438	± 10	0.856	± 1	0.51227	± 0
			10/11/2015	9.75	0.056	0.24	0.723208	± 7	0.854	± 1	-	± -
	RH3		26/08/2015	11.80	0.032	0.18	0.721422	± 12	0.986	± 1	0.51222	± 0
			10/11/2015	12.70	0.033	0.16	0.721169	± 6	0.979	± 1	-	± -

\* Influence of pumping

Table 2:

Type	Name	Depth	Date	SF <sub>6</sub> *	CFC-12				SF <sub>6</sub> *	CFC-12				CFC-12				
					CFC-12	CFC-11	CFC-113	CFC-12		CFC-11	CFC-113	PFM		EMM		BMM		
												Mean age	±**	Mean age	±**	Mix fraction of young component		
					m	pmol/L				pptv			yr	%	yr	%	% (O <sub>2</sub> %***)	%
				x 10 <sup>3</sup>														
Borehole	F5	15	05/05/2015	2.49	3.12	5.53	0.59	6	565	255	87	13	3	5	6	> 99	4	
		15	26/08/2015	5.85	2.25	4.78	0.4	15	408	221	59	30	2	26	<1	75	<1	
	<b>Average</b>											<b>22</b>		<b>16</b>		<b>87</b>		
		23	23/11/2016	5.87	2.48	4.23	0.34	15	449	195	50	29	1	20	<1	82 (88)	<1	
		23	24/04/2018	14.56	0.99	0.34	0.08	16	538	189	53	10	<1	6	2	98 (91)	<1	
		26	26/08/2015	5.43	2.03	3.91	0.33	14	368	181	49	32	<1	32	<1	67	<1	
	<b>Average</b>											<b>24</b>		<b>19</b>		<b>82</b>		
		40	05/05/2015	16.89	1.05	0.97	0.23	43	190	45	34	42	3	86	<1	35	<1	
		40	26/08/2015	11.3	1.36	2.19	0.22	29	247	101	33	40	<1	61	<1	45	<1	
		43	23/11/2016	21.48	0.81	0.56	0.09	55	146	26	13	46	1	124	<1	27 (2)	<1	
		43	24/04/2018	3.61	2.03	0.93	0.2	39	186	16	12	45	5	95	<1	34 (<1)	<1	
	<b>Average</b>											<b>43</b>		<b>92</b>		<b>35</b>		
		F6	63	22/11/2016	5.29	1.35	2.26	0.33	14	244	104	48	41	1	64	<1	45 (60)	<1
			64	25/04/2018	3.14	0.7	1.54	0.16	10	383	45	31	34	1	31	<1	70 (56)	<1
<b>Average</b>											<b>38</b>		<b>48</b>		<b>57</b>			
	F7	45	05/05/2015	1.77	1.03	1.88	0.22	5	187	87	33	42	4	88	<1	34	<1	
		45	26/08/2015	1.59	1.03	1.59	0.17	4	186	73	25	43	1	89	<1	34	<1	
		42	22/11/2016	2.82	1.46	2.69	0.23	7	264	124	34	40	1	57	<1	48 (54)	<1	
		47	22/11/2016	1.46	0.97	1.89	0.16	4	177	87	24	44	5	98	<1	32 (53)	<1	
		47	26/04/2018	5.11	2.58	4.51	0.39	4	253	91	26	42	1	63	<1	46 (53)	<1	
<b>Average</b>											<b>42</b>		<b>79</b>		<b>39</b>			
	F8	27	22/11/2016	4.01	0.76	1.31	0.13	10	137	61	19	47	4	134	<1	25 (20)	<1	
		29	25/04/2018	1.71	1.34	1.89	0.17	8	131	74	25	49	5	145	<1	24 (21)	<1	
<b>Average</b>											<b>48</b>		<b>140</b>		<b>24</b>			
Piezometer	Pz3	11	26/08/2015	5.74	2.31	4.59	0.47	15	419	212	69	29	1	24	<1	77	<1	
		11	22/11/2016	7.29	2.69	4.45	0.33	19	487	206	48	27	<1	15	<1	89 (75)	<1	
	<b>Average</b>											<b>20</b>		<b>15</b>		<b>88</b>		
	Pz5	11	05/05/2015	4.13	3.13	5.52	0.66	11	567	255	97	13	3	5	6	99	4	

	13	23/11/2016	8.27	2.84	4.87	0.36	21	515	225	53	25	<1	11	<1	94 (97)	<1	
	14	24/04/2018	5.98	2.85	3.91	0.34	14	486	218	60	29	1	16	<1	89 (92)	<1	
										<b>Average</b>	<b>22</b>		<b>11</b>		<b>94</b>		
	Pz7	10	05/05/2015	4.18	2.56	6.57	0.58	11	464	304	85	27	<1	18	<1	85	<1
		12	26/08/2015	5.65	2.01	3.66	0.39	15	365	169	57	32	1	32	<1	67	<1
		13	22/11/2016	5.34	2.44	4.33	0.28	14	442	200	41	30	2	21	<1	81 (93)	<1
										<b>Average</b>	<b>30</b>		<b>24</b>		<b>78</b>		
Spring	ARG		05/05/2015	4.12	2.75	5.15	0.67	11	497	238	98						
			26/08/2015	4.68	2.22	4.26	0.41	12	402	197	60						
	CS1		05/05/2015	2.88	2.83	5.45	0.61	7	513	252	89						
			26/08/2015	2.98	2.21	4.24	0.41	8	401	196	61						
	CS2		05/05/2015	6.9	2.99	5.58	0.62	18	541	258	91						
			26/08/2015	4.52	2.44	4.68	0.47	12	442	216	69						
			24/04/2018	-	3.31	5.21	0.45	-	625	252	69						
	CS3		05/05/2015	4.66	2.58	5.37	0.56	12	467	248	82						
			26/08/2015	4.15	2.07	4.11	0.39	11	376	190	58						
	CS4		05/05/2015	3.3	2.98	5.65	0.68	8	540	261	101						
			26/08/2015	4.71	2.31	4.55	0.46	12	418	210	68						
	RH3		26/08/2015	-	2.27	4.21	0.41	-	412	194	61						

\* SF<sub>6</sub> corrected from air excess with Ne concentration (conc.).

\*\* Relative Error (ABS(model conc. - obs conc.)/obs conc.) \* 100.

\*\*\* The value in brackets represents the proportion of recent water estimated with the O<sub>2</sub> values measured in the water (SM Table 6). The maximum value measured in water (8.83mg/L) is used as the current atmospheric value.

Table 3:

Sample name	Number of samples	temperature	Field pH	Conductivity	Na <sup>+</sup>	K <sup>+</sup>	Mg <sup>2+</sup>	Ca <sup>2+</sup>
		°C		20°C µS/cm	mmol/l			
Mean F5 deep*	9	6.6	7.8	214	0.319	0.043	0.385	0.776
Mean F6*	6	6.3	7.8	231	0.134	0.048	0.632	0.719
Mean F7 42m*	5	7.2	7.3	129	0.139	0.043	0.251	0.426
Mean F8 27m*	5	7.3	7.9	161	0.479	0.061	0.184	0.497
Mean Pz3**	10	6.3	5.7	26	0.107	0.016	0.012	0.049
Mean Pz5	9	6.3	5.7	27	0.085	0.015	0.018	0.055
Mean Pz7	10	7.4	5.9	35	0.099	0.032	0.022	0.069
Mean springs Cs	25	6.0	5.7	28	0.086	0.017	0.015	0.063

Sample name	Mn <sup>2+</sup>	Fe <sup>3+</sup>	Al <sup>3+</sup>	Cl <sup>-</sup>	NO <sub>3</sub> <sup>-</sup>	SO <sub>4</sub> <sup>2-</sup>	P total	Si
	mmol/l							
Mean F5 deep*	3.64E-03	6.07E-04	1.21E-04	0.045	0.004	0.065	0.000	0.317
Mean F6*	5.33E-04	1.76E-04	7.55E-05	0.06	0.01	0.063	0.000	0.16
Mean F7 42m*	1.02E-04	3.37E-04	1.19E-04	0.054	0.056	0.059	0.003	0.271
Mean F8 27m*	2.73E-05	1.22E-04	1.84E-04	0.048	0.027	0.036	0.001	0.306
Mean Pz3 surface**	1.30E-04	2.40E-04	1.73E-03	0.035	0.032	0.041	0.002	0.195
Mean Pz5	2.08E-04	4.45E-04	1.04E-03	0.039	0.037	0.05	0.001	0.159
Mean Pz7	2.58E-04	3.58E-04	2.59E-03	0.042	0.091	0.05	0.002	0.181
Mean springs Cs	0.000	4.01E-04	1.44E-03	0.040	0.072	0.042	0.002	0.156

\* Average of concentration without the sample from 10/01/18

\*\* Pz3 average concentration without the three deepest charged samples

Table 4:

Sample	Saturation index												
	Quartz	Albite	K-Feldspar	Anorthite	Apatite	Kaolinite	Illite	Muscovite	Montmorillonite	Calcite	Dolomite	Biotite	Andrydrite
Mean F5 deep	0.862	0.571	3.041	-4.12	-9.957	4.687	4.35	5.037	3.161	-0.339	0.299	4.104	-3.342
Mean F6	0.572	-0.879	2.021	-5.153	-10.309	3.717	2.958	3.632	1.78	-0.337	0.545	1.364	-3.402
Mean F7 42m	0.782	-0.278	2.542	-4.996	-15.015	4.992	4.037	4.996	2.665	-1.335	-1.161	0.469	-3.571
Mean F8 27m	0.834	0.858	3.29	-3.929	-11.253	4.791	4.582	5.443	3.283	-0.537	-0.215	-8.643	-3.732
Mean Pz3	0.659	-2.472	0.049	-9.611	-33.426	4.54	1.014	2.309	-0.533	-5.139	-9.619	-17.544	-4.542
Mean Pz5	0.57	-3.058	-0.465	-10.18	-37.179	3.921	0.223	1.353	-1.223	-5.102	-9.42	-17.253	-4.408
Mean Pz7	0.603	-1.919	0.916	-8.024	-39.704	5.489	2.536	4.223	0.717	-4.757	-8.72	-15.455	-4.31
Mean spring	0.536	-2.713	-0.066	-9.25	-40.603	4.492	1.022	2.378	-0.591	-4.967	-9.221	-16.583	-4.392

Table 5:

<b>Borehole</b>	<b>F6</b>	<b>F7</b>	<b>F8</b>	<b>F5</b>
Sampling depth* (m)	63	42 - 47	26	45
Longest way**(m)	100	300	430	730
EMM mean age (yr)	31 - 64	57 - 98	134 - 145	61 - 124
Velocity vertical (m/yr)	0.98 - 2.03	0.42 – 0.82	0.18 – 0.19	0.36 – 0.74
Velocity longest way (m/yr)	1.56 - 3.23	3.06 – 5.26	2.97 – 3.21	5.89 – 11.97

\* Corresponding to input area from fracture network

\*\* Distance from the top added to the sampling depth

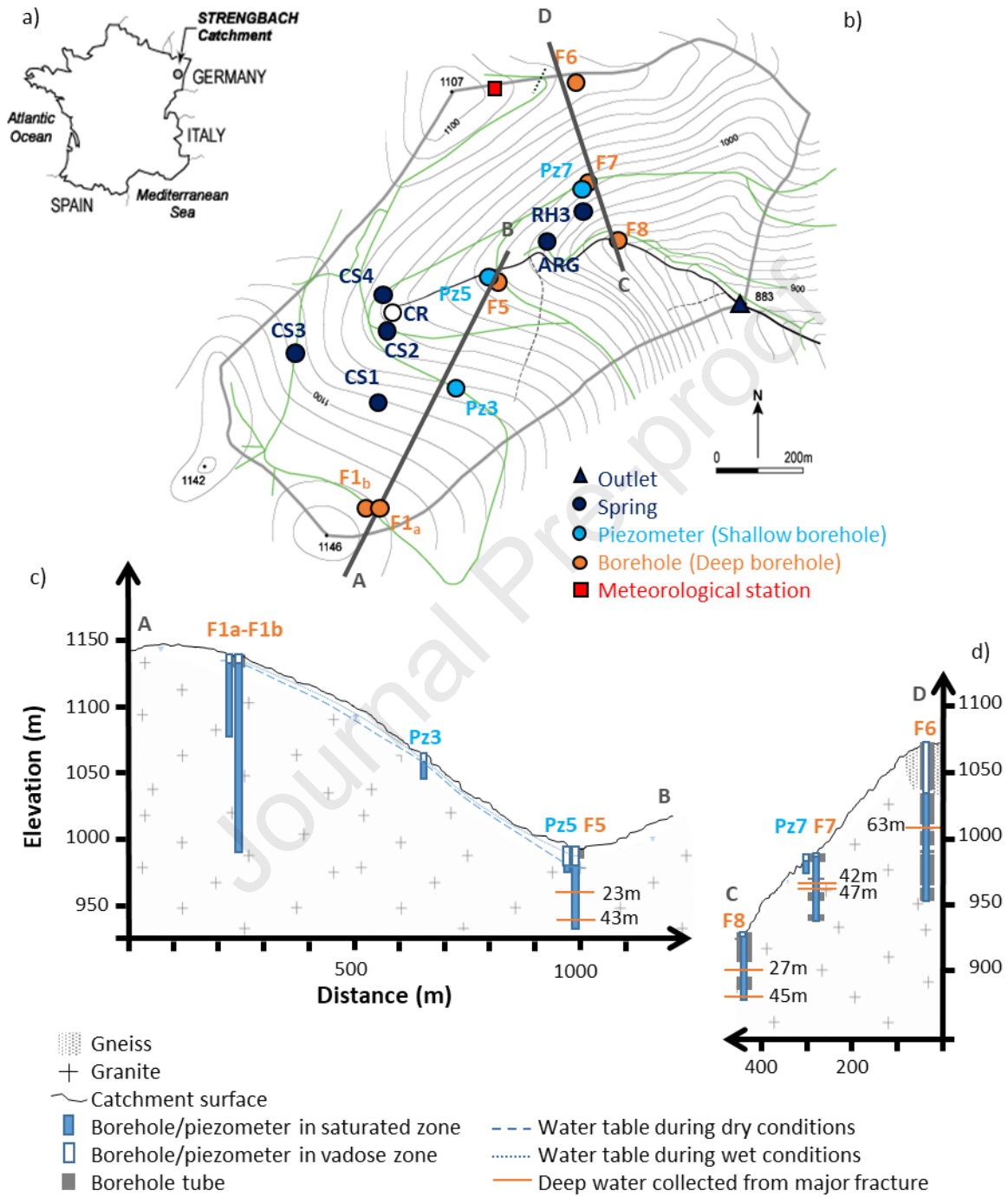


Figure 1:

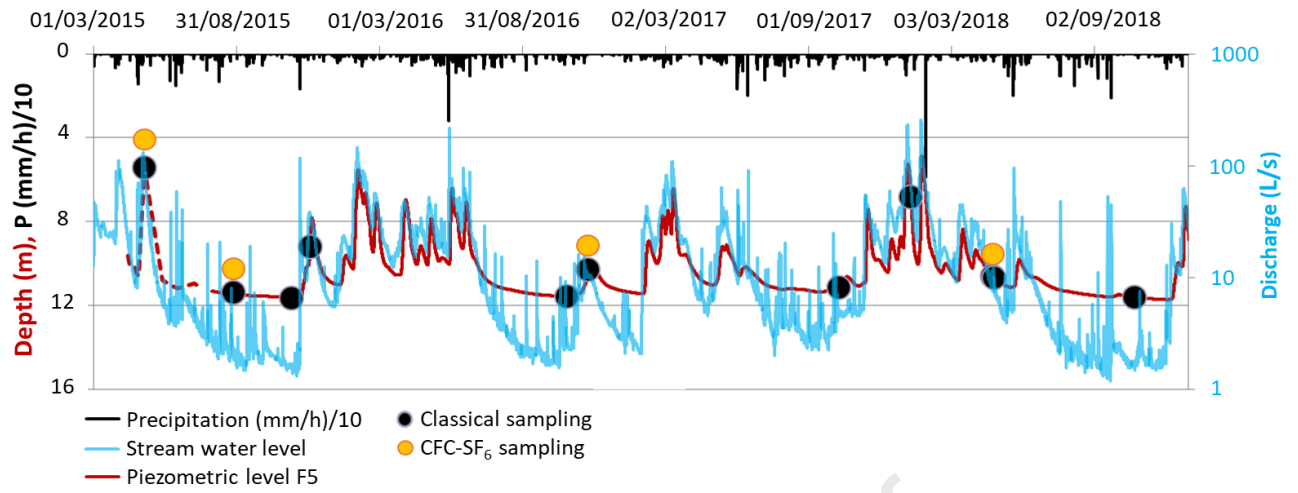


Figure 2

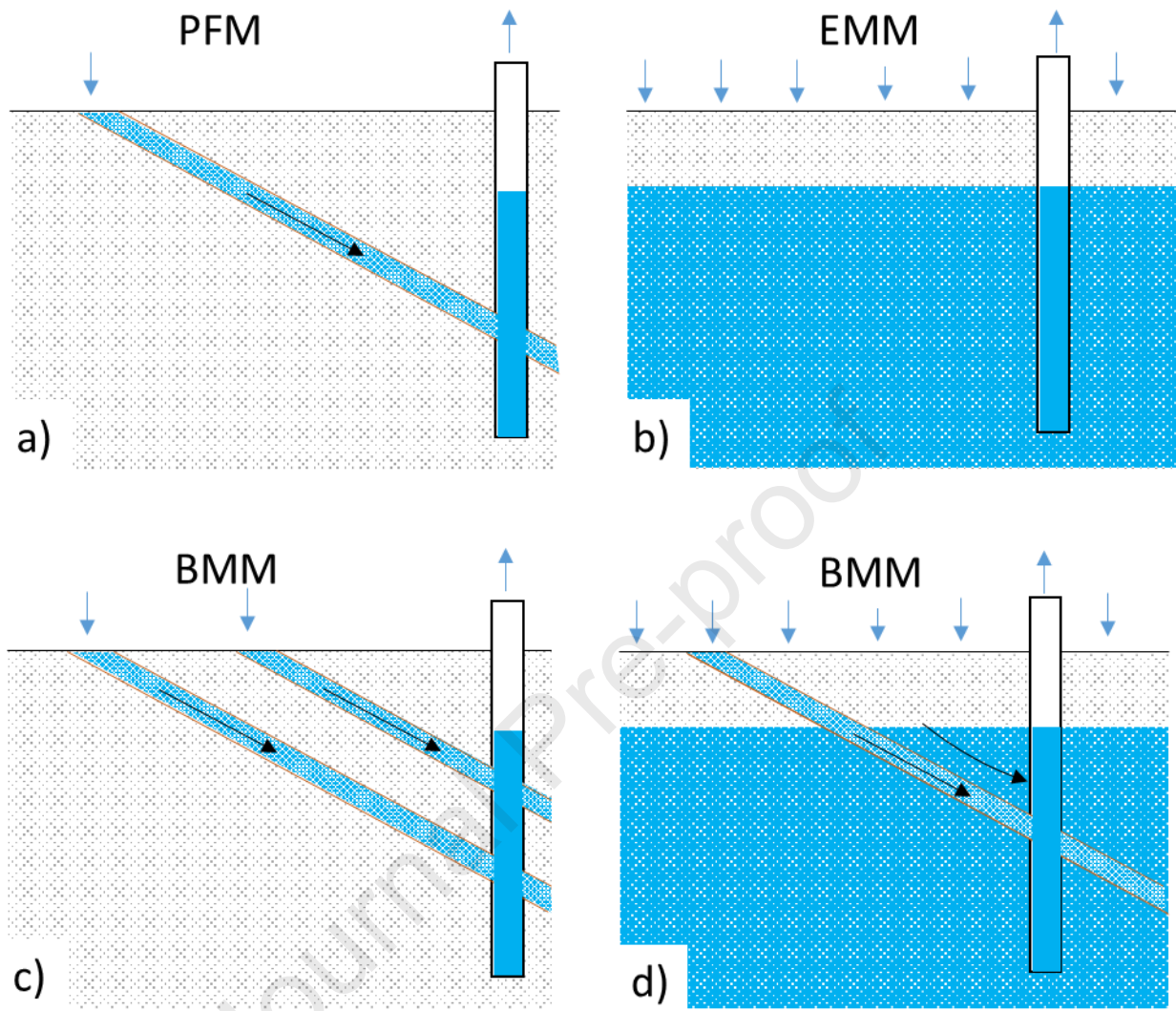


Figure 3

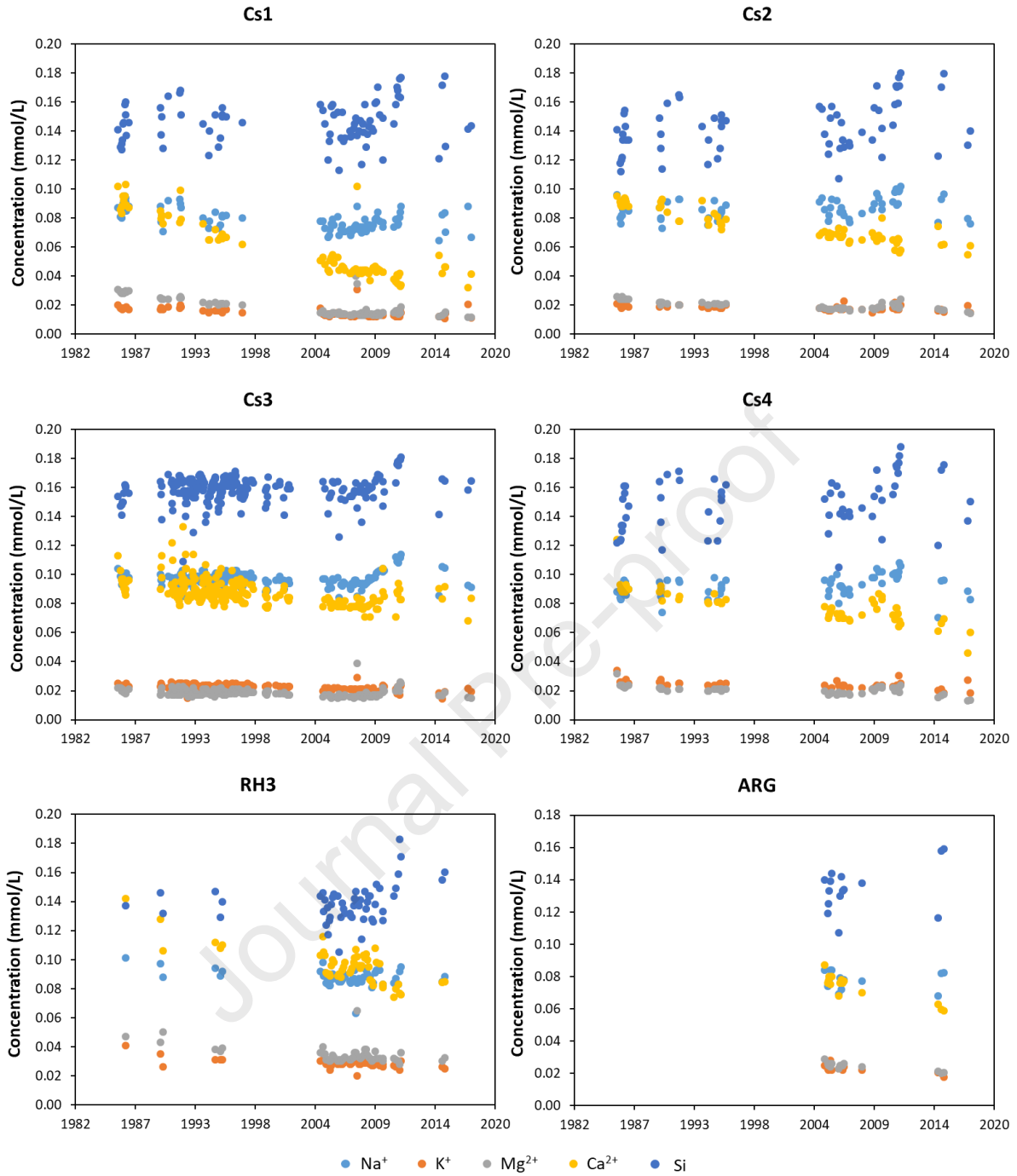


Figure 4

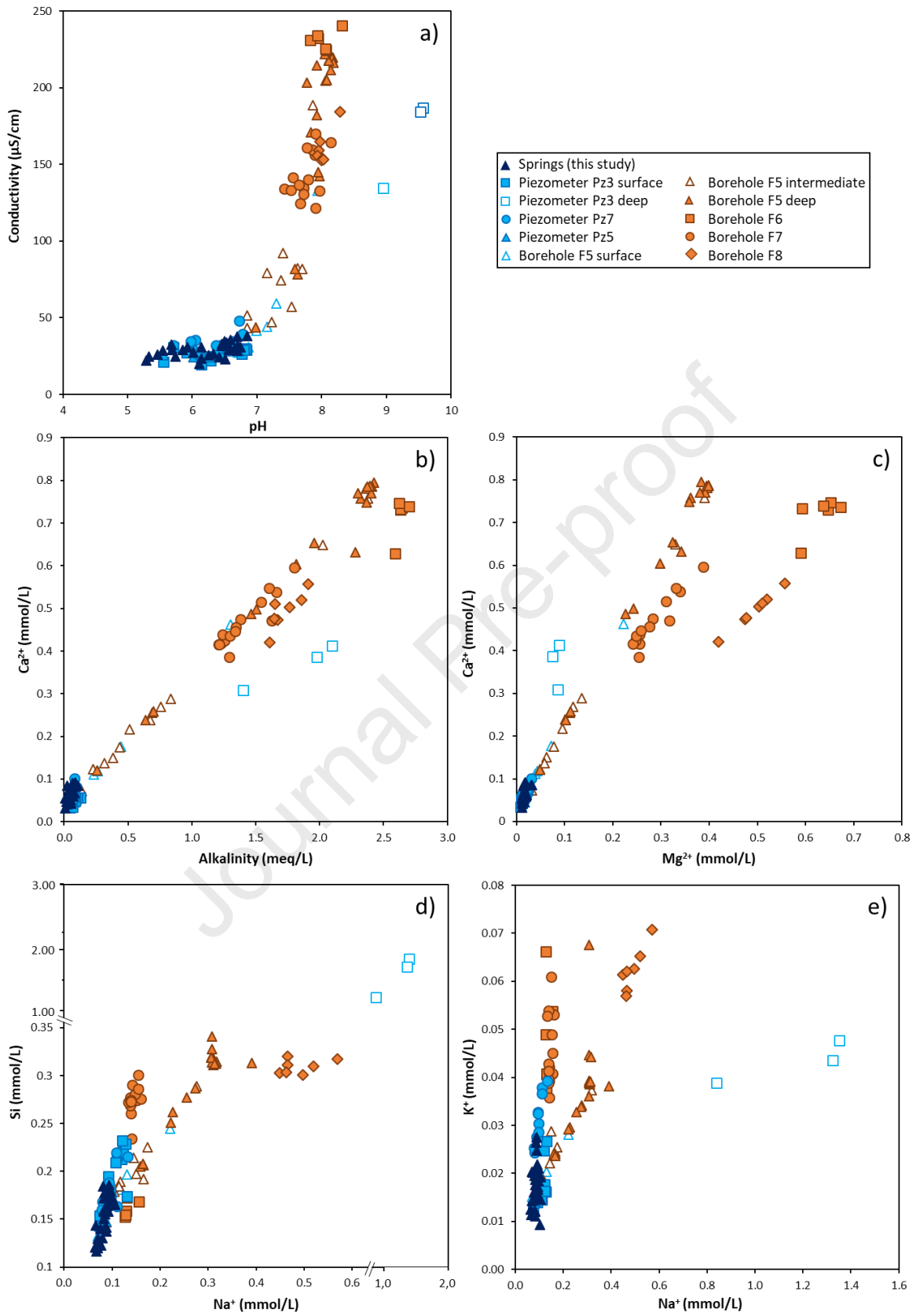


Figure 5

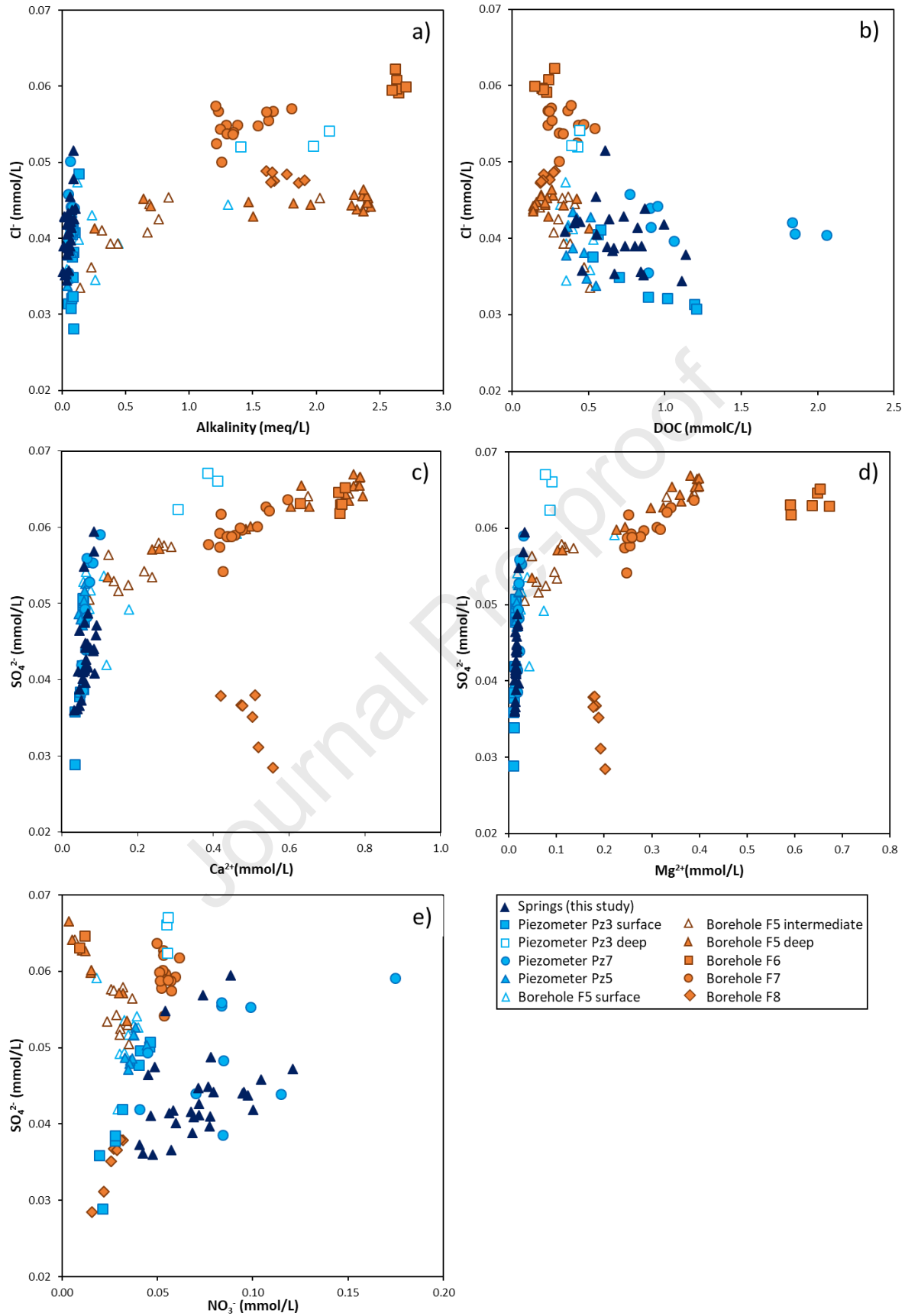


Figure 6

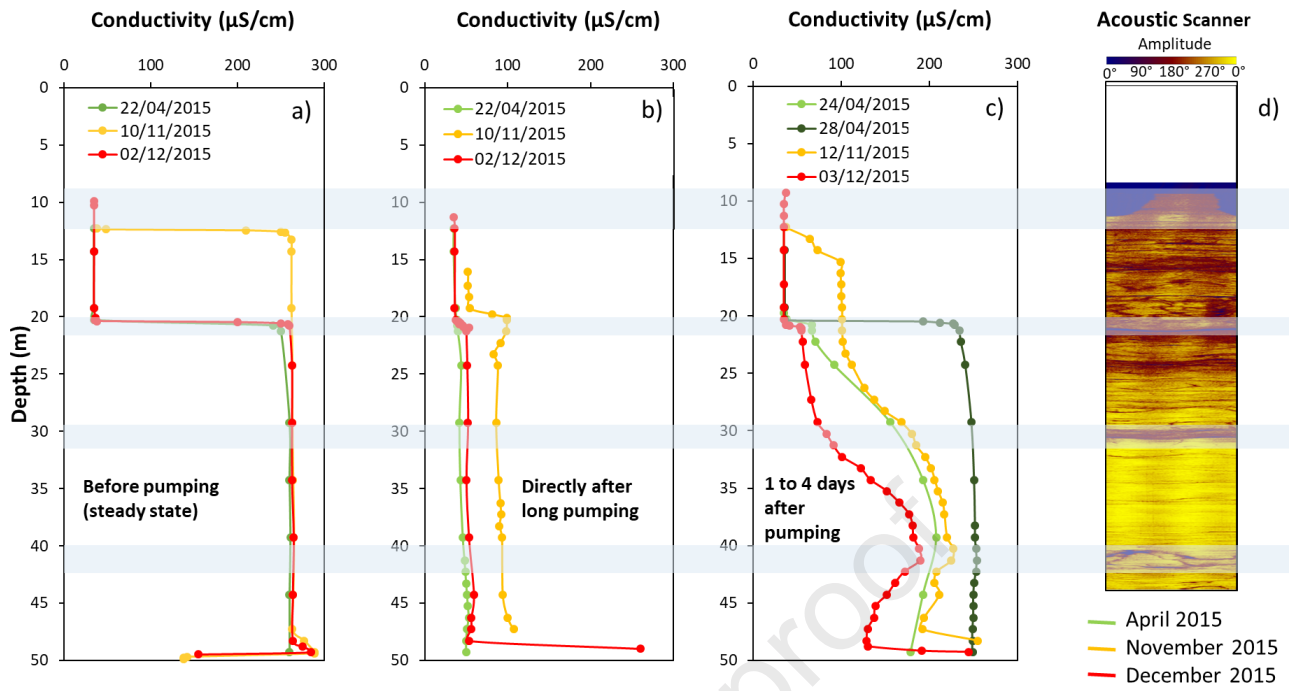


Figure 7

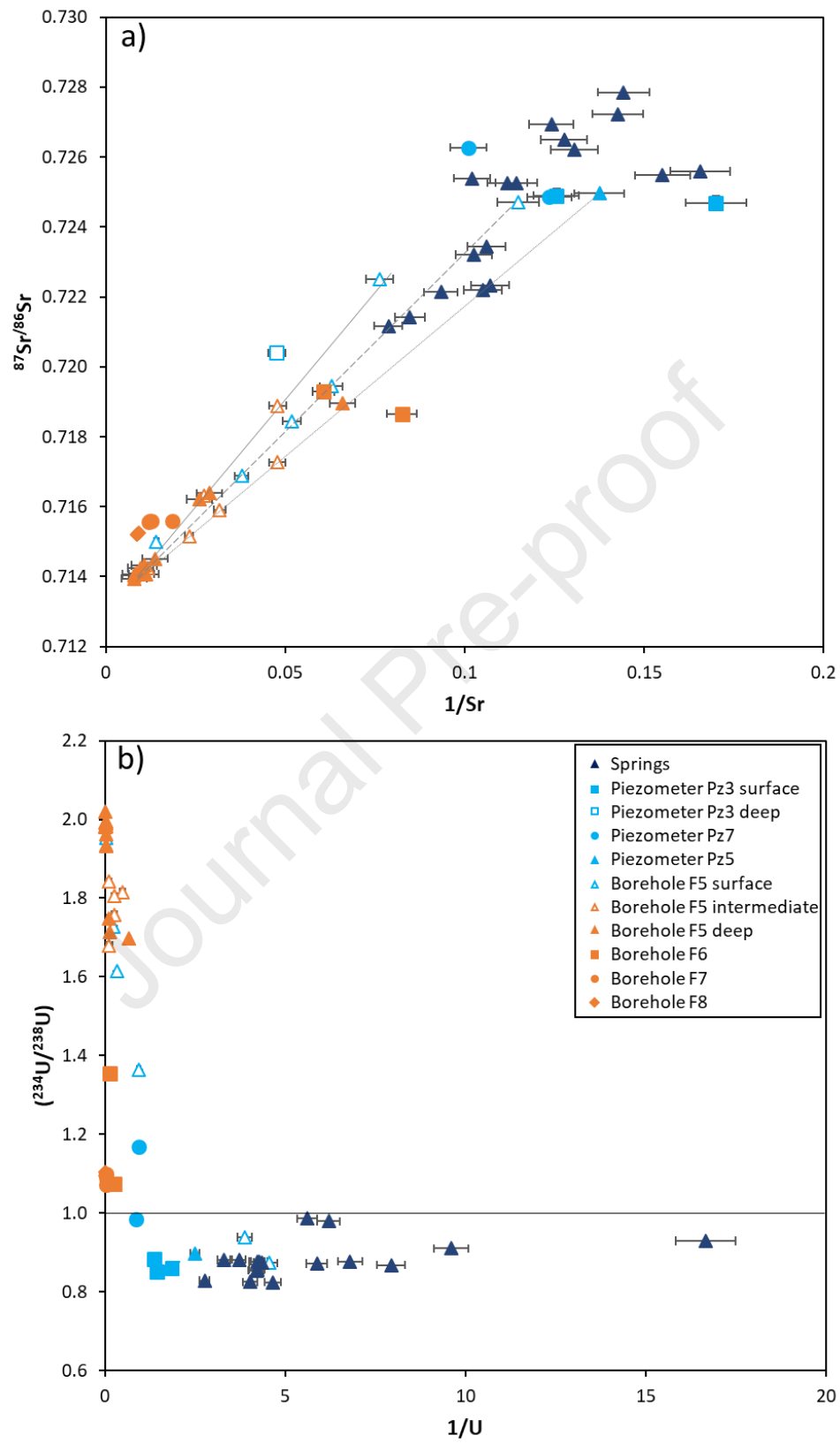


Figure 8

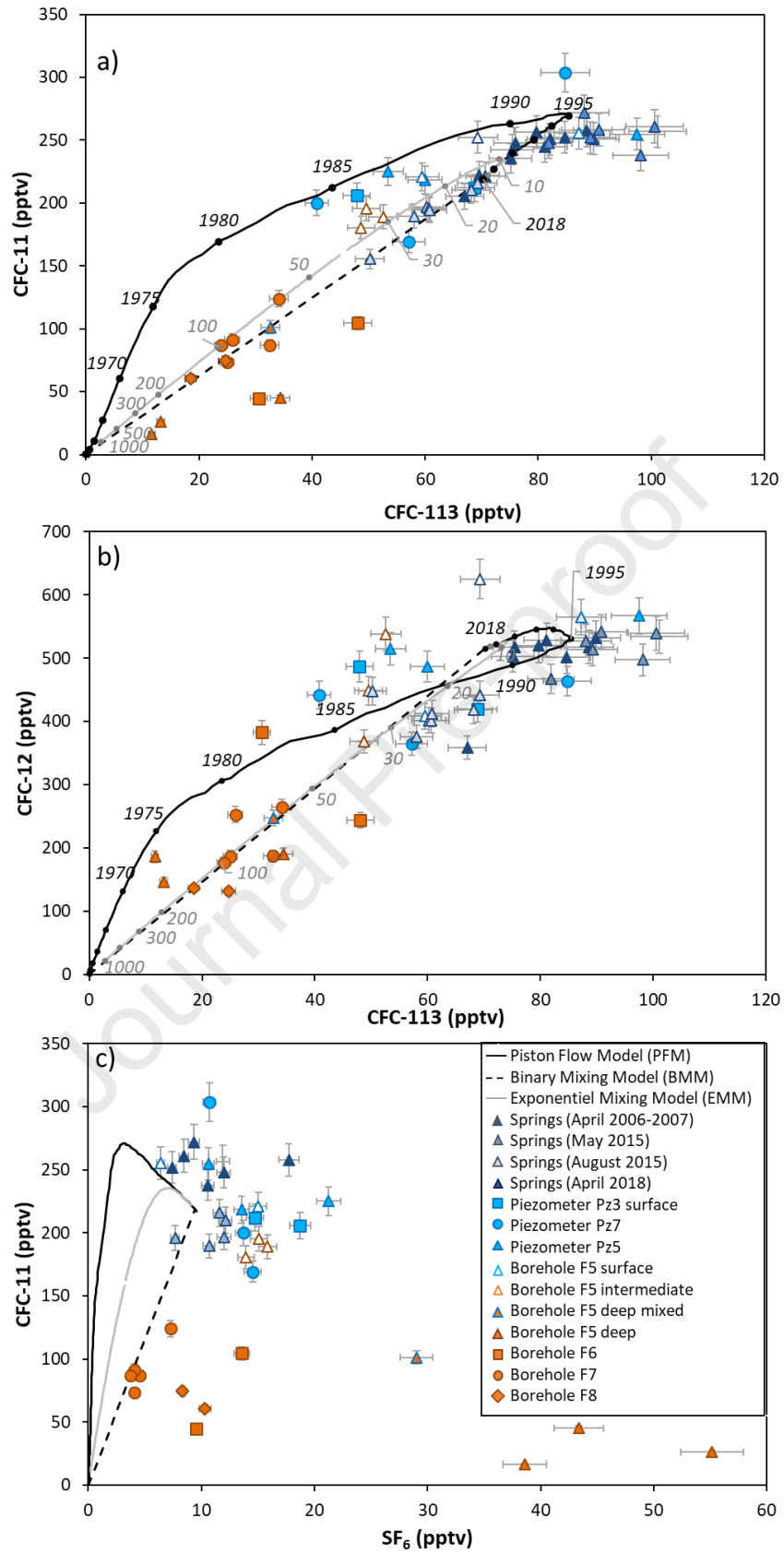


Figure 9

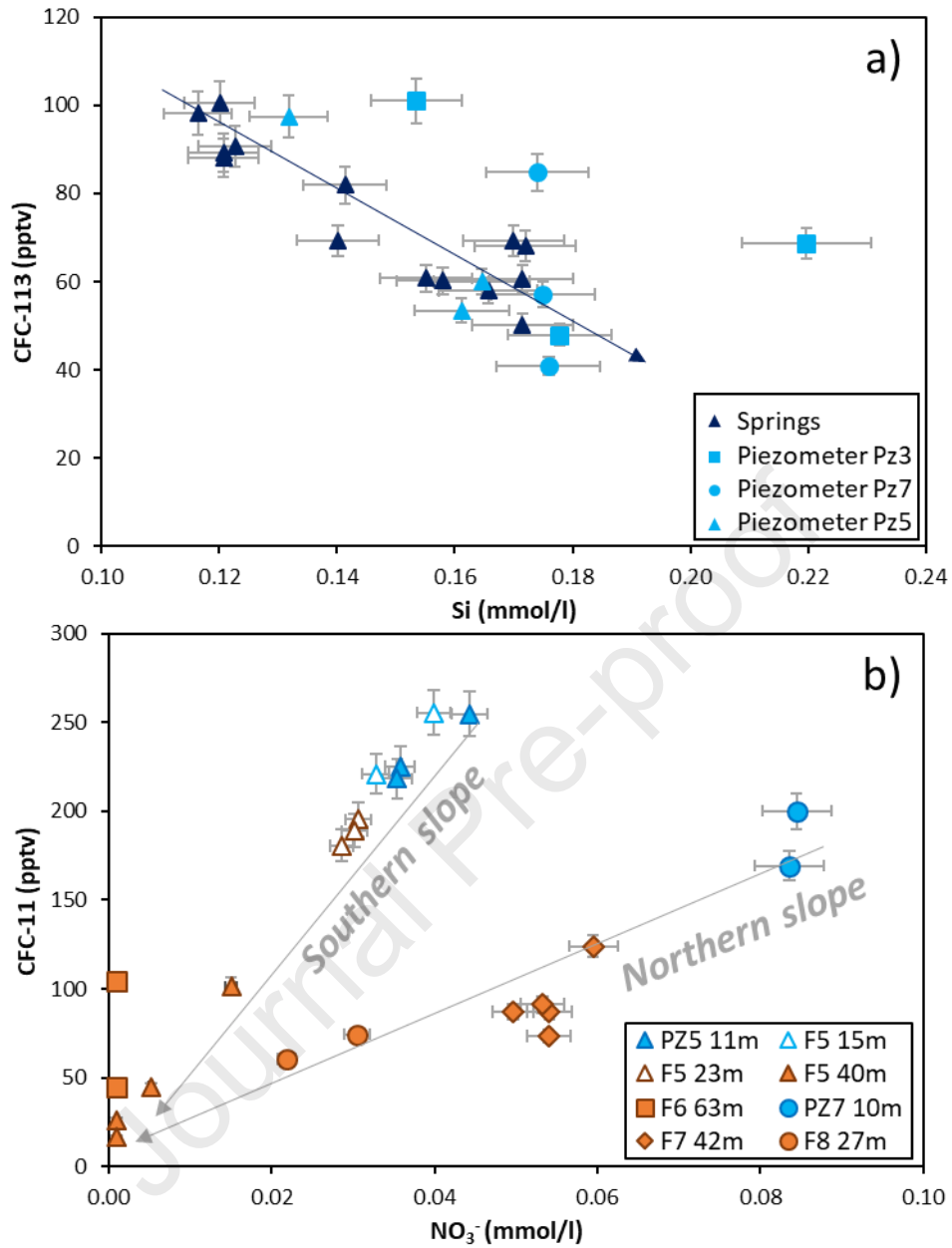


Figure 10

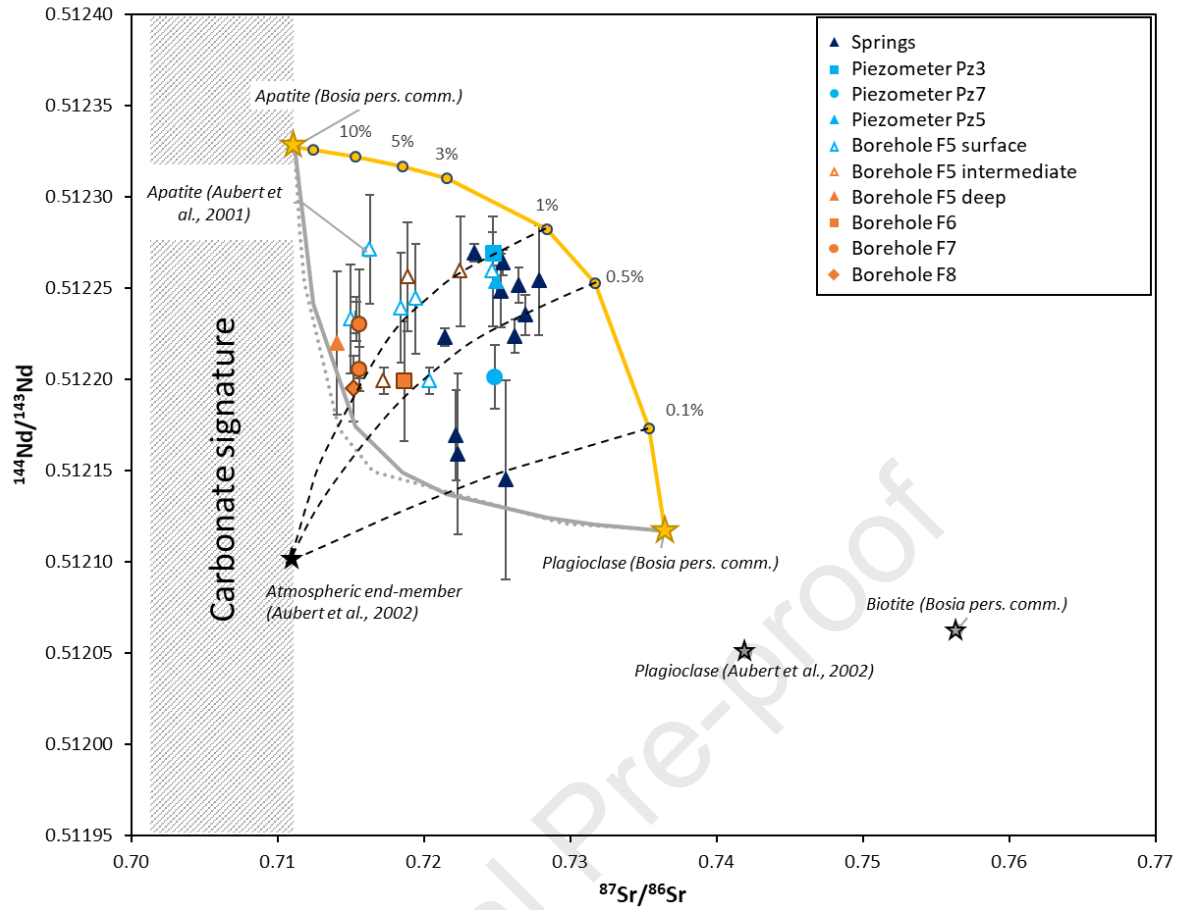


Figure 11

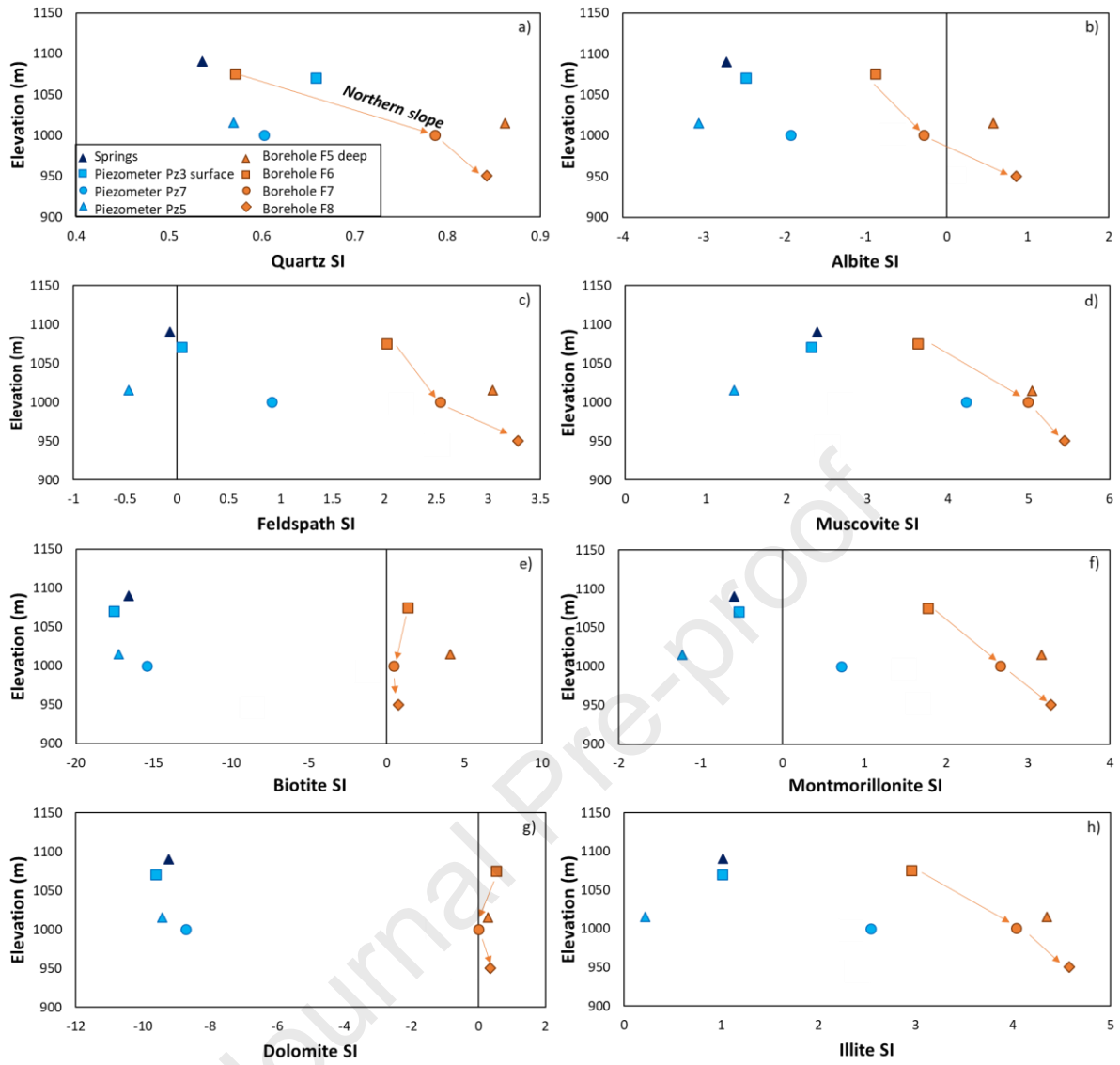


Figure 12

Highlights :

- Geochemical typology of deep water in the Strengbach critical zone observatory
- Specific chemical concentrations and Sr-U isotope ratios relative to surface water
- Evidence of longer residence times (water ages > 50 years) for the deep water
- Different circulation histories for surface and deep water in the Strengbach CZO

Journal Pre-proof

**Declaration of interests**

The authors declare that they have no known competing financial interests or personal relationships that could have appeared to influence the work reported in this paper.

The authors declare the following financial interests/personal relationships which may be considered as potential competing interests:

Journal Pre-proof